Optical Spatial Modulation for FSO IM/DD Communications with Photon-Counting Receivers: Performance Analysis, Transmit Diversity Order and Aperture Selection

Chadi Abou-Rjeily, *Senior Member IEEE,* and Georges Kaddoum, *Member IEEE*

***Abstract*—This paper investigates two pulse-based Optical Spatial Modulation (OSM) schemes as cost-efficient solutions for multi-aperture Free-Space Optical (FSO) communications with Intensity-Modulation and Direct-Detection (IM/DD). Namely, we consider Optical Space Shift Keying (OSSK) where information is encoded in the index of the pulsed optical source and Spatial Pulse Position Modulation (SPPM) where additional bits determine the position of the transmitted optical pulse resulting in higher transmission rates. A performance analysis is carried out over gamma-gamma channels with the exact Poisson photon-counting detection model. Exact Symbol Error Probability (SEP) expressions, simple upper bounds and the achievable transmit diversity orders are derived for both the open-loop and closed-loop scenarios. Based on the presented performance analysis, a transmit aperture selection scheme capable of maximizing the transmit diversity order is proposed for OSSK and SPPM in the closed-loop case. Results show that for open-loop OSSK, open-loop SPPM and closed-loop OSSK, the transmit diversity order does not depend on the severity of scintillation unlike the closed-loop SPPM case.**

***Index Terms*—Free-Space Optics, Multiple-Input-Multiple-Output, Optical Spatial Modulation, OSM, performance analysis, diversity order, aperture selection, open-loop, closed-loop.**

.

I. Introduction

Spatial Modulation (SM) is attracting an increased interest as a low-complexity energy-efficient Multiple-Input-Multiple-Output (MIMO) solution [1], [2]. By activating a single transmit antenna at a time, SM avoids inter-channel interference at the receiver and alleviates the need for inter-antenna synchronisation at the transmitter thus circumventing many of the complexity and cost drawbacks often associated with the other MIMO techniques. On the other hand, by mapping a part of the information bits to the antenna index, attractive multiplexing gains can be achieved compared to single-antenna systems [1], [2]. SM can be implemented either in the open-loop or closed-loop setups. While the open-loop scenario does not result in any transmit diversity gains [3], [4], such gains can be achieved by implementing the closed-loop alternative [5]–[8]. The Euclidean Distance optimized Antenna Selection (EDAS) constitutes an appealing solution that has been investigated extensively in the literature [5]–[8]. For Radio Frequency (RF) systems subject to Rayleigh fading and corrupted by Additive White Gaussian Noise (AWGN), it has been proven that the EDAS scheme increases the transmit diversity order from 1 in the open-loop scenario [3], [4] to $(P - P_s + 1)$ where P is the total number of transmit antennas and P_s is the number of selected transmit antennas [5]. The research targeting the RF-SM-EDAS systems revolved around the complexity reduction of the antenna selection scheme in the contexts of conventional [7] and large-scale [8] MIMO systems.

On the other hand, the ever-increasing demand for bandwidth motivated researchers to investigate the optical spectrum as a means to complement the crowded RF spectrum. In this context, Optical Wireless Communications (OWC) emerged as a promising technology for the next generation high-speed wireless communications for both the indoor and outdoor scenarios. Consequently, a new direction of research has surfaced corresponding to the extension of the RF-SM techniques to the context of OWC which is also referred to as Optical-SM (OSM) in the literature [9]. As such, recent research revolved around the application of OSM for indoor Visible Light Communications (VLC) [9]–[14] and for outdoor Free-Space Optical (FSO) communications [15]–[20]. In [9], the bit error rate (BER) analysis of OSM was carried out over indoor optical channels highlighting the impact of the channel correlation on the achievable performance levels. OSM was compared with Spatial Multiplexing (SMux) and Repetition Coding (RC) in [10] showing that OSM is more robust against channel correlation compared to SMux while enhancing the spectral efficiency compared to RC. Adaptive VLC-OSM solutions were proposed in [11] and [12] based on adapting the Pulse Amplitude Modulation (PAM) modulation-orders at the light-emitting diodes (LEDs) and on implementing channel-adaptive bit mapping, respectively. Finally, an adaptive power allocation strategy was proposed in [13] for solving the mobility problem in VLC-OSM systems. More recently, the effect of inter-symbol interference on the performance of OSM over indoor multi-path channels was investigated in [14]. In [14], two variants of OSM were considered; namely, the Optical Space Shift Keying (OSSK) and Spatial Pulse Position Modulation (SPPM). OSSK constitutes an OWC-adapted extension of the RF-SSK solution that constitutes a special form of RF-SM where the information is conveyed only in the antenna space with no modulation. In other words, in OSSK, the

Chadi Abou-Rjeily is with the Department of Electrical and Computer Engineering of the Lebanese American University (LAU), PO box 36 Byblos 961, Lebanon. (e-mail: chadi.abourjeily@lau.edu.lb).

Georges Kaddoum is with University of Québec, ÉTS engineering school, LACIME Laboratory, Montreal, Canada (email: georges.kaddoum@etsmtl.ca).

information is conveyed in the index of the pulsed LED thus transmitting $\log_2(P)$ bits per symbol duration. On the other hand, for SPPM, the bits are mapped to the LED index and to the position index of an M-ary PPM constellation thus transmitting $\log_2(M)$ additional bits compared to OSSK.

Compared to the indoor VLC channels, the outdoor FSO channels do not suffer from excessive delay spreads (multi-path propagation) or pronounced channel correlation. On the other hand, FSO systems suffer from scintillation resulting in the random fluctuation of the received signal power in a phenomenon that is analogous to fading over RF wireless channels. Consequently, the MIMO techniques found direct application in FSO systems where RC [21] and SMux [22] constitute the most commonly adopted solutions. To leverage the limited spectral efficiency of RC (that transmits at the same rate as single-aperture systems) and the decoding complexity associated with SMux (where the P transmitted independent data streams need to be jointly detected), there has been a growing interest in studying FSO-OSM systems [15]–[20]. Open-loop OSSK with Intensity-Modulation and Direct-Detection (IM/DD) constitutes the most widely investigated OSM scheme [15]–[17]. Multiple-Input-Single-Output (MISO) FSO-OSSK systems were analyzed in [15] over gamma-gamma channels with pointing errors. MIMO FSO-OSSK systems were studied in [16] over gamma-gamma channels with no pointing errors and in [17] over gamma-gamma, lognormal and negative exponential channels with pointing errors. The works in [15]–[17] revolved around evaluating the distribution of the difference between two path gains and were culminated by deriving the transmit diversity order that was found to be equal to $1/2$ independently from the scintillation and pointing error conditions. Open-loop FSO-OSM with joint PAM-PPM constellations and IM/DD was investigated in [18] over gamma-gamma and lognormal scintillation. Jointly encoding the positions and amplitudes of the transmitted optical pulses enhances the spectral efficiency compared to OSSK. While in [18] a theoretical framework for deriving bounds on the error probability was developed, the so-called type-IV error that involves the difference between two gamma-gamma random variables was evaluated numerically with the consequence that the achievable diversity order was not ascertained theoretically. While the solutions in [15]–[18] considered non-coherent IM/DD communications, the work in [19] considered open-loop FSO-OSSK systems with coherent heterodyne receivers over H-K atmospheric turbulence channels. In [19], it was proven that a transmit diversity order of 1 can be achieved independently from the fading severity. Finally, the performance of subcarrier intensity modulation OSM systems was evaluated numerically in [20] over lognormal outdoor channels.

This work targets the performance analysis of MISO FSO-OSSK and FSO-SPPM IM/DD systems over gamma-gamma atmospheric turbulence channels in the open-loop and closed-loop scenarios. Unlike all existing works on VLC-OSM [9]–[14] and FSO-OSM [15]–[20] that consider the AWGN model, this work adopts the exact Poisson photon-counting detection model where the number of photons generated by the optical signal and by the background radiation is modeled by a Poisson point process [21]–[24]. This constitutes the major novelty of this work since the performance of OSM systems with Poisson noise was never considered before in the literature. It is worth noting that the Poisson model constitutes the exact noise model describing the performance of IM/DD systems while the simpler AWGN model constitutes an approximation that holds when the shot noise caused by background radiation is dominant with respect to the other noise components such as thermal noise and dark currents [21]–[24].

This work differentiates itself from all previous works on FSO-OSM [15]–[20] by the following. i): Unlike [15]–[20] that consider the approximate AWGN model, this work considers the more general Poisson model. ii): Unlike [15]–[20] that all consider the open-loop scenario, this work addresses the open-loop as well as the closed-loop scenarios. iii): Considering the pervious FSO-OSM works examining gamma-gamma scintillation [15]–[17], this work analyzes not only OSSK but SPPM as well. iv): While [18] evaluates the performance of FSO-OSM with joint PAM-PPM over gamma-gamma channels numerically, a closed-form theoretical evaluation is carried out in this paper. Moreover, unlike [18], the achievable transmit diversity orders are handily quantified.

The contributions of this paper are fourfold:

- We derive exact SEP expressions and simple bounds for OSSK and SPPM. The derived expressions are novel and the bounds are useful for offering clear and intuitive insights on the performance of FSO OSM systems.
- We prove that the transmit diversity order achieved by OSSK in the open-loop scenario is equal to $1/2$. This result, obtained under the Poisson noise model, matches the result obtained in [15]–[17] under the AWGN model. For SPPM, we prove that the diversity order is equal to $\min\{\beta, \frac{1}{2}\}$ where β is the parameter of the gamma-gamma distribution. For practical values of the link distance and scintillation severity, this latter quantity simplifies to $1/2$ as in the case of OSSK. The novelty in evaluating the diversity order in the open-loop scenario revolves around adopting a recent technique based on approximating the gamma-gamma distribution by a mixture gamma distribution over the entire range of irradiances.
- We evaluate the transmit diversity order that can be achieved in the closed-loop scenario based on the strengths of the channel irradiances. This evaluation follows from analyzing the distribution of the difference between the square-roots of two order statistics among the sorted gamma-gamma random variables. As in the open-loop scenario, the novelty of the adopted calculation methodology yielded conclusive closed-form results.
- We propose a novel diversity-maximizing transmit aperture selection scheme for the closed-loop scenario. For OSSK, the proposed scheme achieves a transmit diversity order of $\frac{1}{2}\left\lfloor \frac{P-1}{P_s-1} \right\rfloor$ when activating P_s apertures out of the P available transmit apertures. For SPPM, the achievable transmit diversity order is equal to $\max\left\{\frac{1}{2}\tilde{k}, [P-(\tilde{k}+1)(P_s-1)]\beta\right\}$ where $\tilde{k} = \left\lfloor \frac{2P\beta}{1+2(P_s-1)\beta} \right\rfloor$. The proposed aperture selection scheme is completely novel and adapted to FSO IM/DD systems.

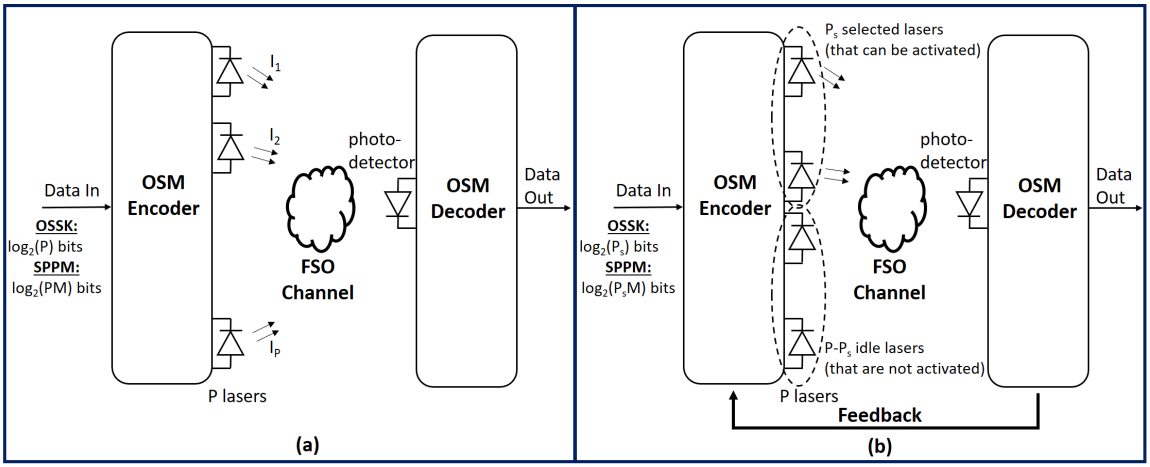

Fig. 1. $P \times 1$ FSO OSM system model. (a): Open-Loop scenario and (b): Closed-Loop scenario.

II. System Model

A. Basic Parameters

Consider a $P \times 1$ FSO communication system where the transmitter is equipped with P transmit apertures (lasers) while the receiver is equipped with a single receive aperture (photo-detector). The system model is better depicted in Fig. 1 in the open-loop and closed-loop scenarios. We assume that the P optical channels are independent and identically-distributed according to the gamma-gamma distribution whose probability density function (pdf) is given by [16]:

$$f_I(I) = \frac{2(\alpha\beta)^{\frac{\alpha+\beta}{2}}}{\Gamma(\alpha)\Gamma(\beta)} I^{\frac{\alpha+\beta}{2}-1} K_{\alpha-\beta}\left(2\sqrt{\alpha\beta I}\right) \;\; ; \;\; I \geq 0, \quad (1)$$

where $\Gamma(\cdot)$ is the Gamma function and $K_c(\cdot)$ is the modified Bessel function of the second kind of order c. In (1), the channel parameters α and β are the effective numbers of small-scale and large-scale eddies that can be expressed, for spherical wave propagation, as $\alpha = \left[\exp\left(0.49\sigma_R^2/(1+1.11\sigma_R^{12/5})^{7/6}\right) - 1\right]^{-1}$ and $\beta = \left[\exp\left(0.51\sigma_R^2/(1+0.69\sigma_R^{12/5})^{5/6}\right) - 1\right]^{-1}$ [15]. The parameters α and β depend on the link distance d through the Rytov variance $\sigma_R^2 = 1.23 C_n^2 k^{7/6} d^{11/6}$ where k is the wave number and C_n^2 denotes the refractive index structure parameter. For terrestrial FSO links, C_n^2 ranges from 10^{-17} $\text{m}^{-2/3}$ for weak turbulence to 10^{-12} $\text{m}^{-2/3}$ for strong turbulence. In this work, unless stated otherwise, we fix $C_n^2 = 1.7 \times 10^{-14}$ $\text{m}^{-2/3}$ corresponding to the scenario of average turbulence [15].

The receiver is an IM/DD photon-counting receiver. Denote by λ_s and λ_b the average numbers of electrons generated by the information-carrying signal, in the absence of scintillation, and by the background radiation and dark currents, respectively. These quantities are given by [22]:

$$\lambda_s = \eta \frac{E_s}{hf} \quad ; \quad \lambda_b = \eta \frac{E_b}{hf}, \quad (2)$$

where η is the detector's quantum efficiency, h is Planck's constant and f is the optical center frequency corresponding to a wavelength of 1550 nm. In (2), E_s and E_b denote the received optical energies resulting from the light signal and background radiation, respectively.

We denote by M the number of time slots per symbol duration. For SPPM, M corresponds to the number of PPM positions while, for OSSK, $M = 1$ reflecting the fact that the transmitted optical pulse occupies the entire symbol duration. For SPPM, one of the P transmit apertures is pulsed in a single PPM slot (out of the M available slots) resulting in the transmission rate of $\log_2(MP)$ bits per channel use (bpcu). In this case, the transmitted constellation is given by the set $\{s_{p,m} \in \{0,1\} \; ; \; p = 1,\ldots,P \; , \; m = 1,\ldots,M\}$ where $s_{p,m} = 1$ (resp. $s_{p,m} = 0$) indicates that the p-th transmit aperture is pulsed (resp. not pulsed) in the m-th PPM position. One of the elements of the vector $[s_{1,1},\ldots,s_{1,M}\cdots s_{P,1},\ldots,s_{P,M}]$ is equal to 1 while the remaining $MP-1$ elements are equal to 0. For OSSK, the information is completely conveyed by the index of the pulsed transmit aperture resulting in the rate of $\log_2(P)$ bpcu. In what follows, for the sake of a unified notation, OSSK will be handled as a special case of SPPM obtained by setting $M = 1$. Following from the unified notation, the energies in (2) can be expressed as $E_s = P_s \frac{T_s}{M}$ and $E_b = P_b \frac{T_s}{M}$ where T_s stands for the symbol duration while P_s and P_b stand for the incident optical power and the power of background noise, respectively. In this work, all reported error rates will be plotted as a function of the signal energy per information bit given by $\frac{E_s}{\log_2(MP)}$ for the sake of fairness when comparing systems with different rates. Moreover, we set $E_b = -185$ dBJ for all of the presented numerical results.

Considering the generic exact Poisson photon-counting detection model [21]–[24], the detection at the receiver is based on the M decision variables $\{R_m\}_{m=1}^{M}$ where R_m stands for the number of photo-electrons detected in the m-th slot[1]. The random variable R_m follows the Poisson distribution with the following parameter [22]:

$$\mathrm{E}\left[R_m\right] = \left[\sum_{p'=1}^{P} s_{p',m} I_{p'}\right] \lambda_s + \lambda_b \;\; ; \;\; m = 1,\ldots,M, \quad (3)$$

[1]For OSSK, a single decision variable R_1 is needed corresponding to the number of photo-electrons detected over T_s.

where $\mathrm{E}[\cdot]$ stands for the averaging operator while I_p stands for the channel irradiance from the p-th transmit aperture to the receive aperture. For OSM where a single transmit aperture is pulsed per symbol duration, only one term in the summation in (3) will be different from zero. In other words, when the transmit aperture p is pulsed in the m-th slot (i.e. $s_{p,m}=1$), R_m will have a mean of $I_p\lambda_s+\lambda_b$ while the remaining $M-1$ decision variables $\{R_{m'}\ ;\ m'\neq m\}_{m'=1}^{M}$ will have a mean of λ_b showing that the only source of photo-electrons in these empty slots is background radiation[2].

B. Maximum-Likelihood (ML) Detection

Denote by $[r_1,\ldots,r_M]$ the actual numbers of photo-electrons detected in the M slots. The ML decoder decides in favor of $s_{\hat{p},\hat{m}} = \arg\max_{p=1,\ldots,P\ ;\ m=1,\ldots,M}\Pr\left(R_1=r_1,\ldots,R_M=r_M|s_{p,m}\right)$ that, from (3), results in:

$$s_{\hat{p},\hat{m}} = \underset{\substack{p=1,\ldots,P\\ m=1,\ldots,M}}{\arg\max}\left\{\frac{e^{-(I_p\lambda_s+\lambda_b)}(I_p\lambda_s+\lambda_b)^{r_m}}{r_m!}\prod_{\substack{m'=1\\ m'\neq m}}^{M}\frac{e^{-\lambda_b}\lambda_b^{r_{m'}}}{r_{m'}!}\right\} \tag{4}$$

$$= \underset{\substack{p=1,\ldots,P\\ m=1,\ldots,M}}{\arg\max}\left\{e^{-I_p\lambda_s}\left(1+\frac{I_p\lambda_s}{\lambda_b}\right)^{r_m}\prod_{m'=1}^{M}\frac{e^{-\lambda_b}\lambda_b^{r_{m'}}}{r_{m'}!}\right\}. \tag{5}$$

Removing the last term from (5) that does not depend on p or m while taking the logarithm of the probability results in the following equivalent ML decision rule:

$$s_{\hat{p},\hat{m}} = \underset{p=1,\ldots,P\ ;\ m=1,\ldots,M}{\arg\max}\left\{r_m\log\left(1+\frac{I_p\lambda_s}{\lambda_b}\right)-I_p\lambda_s\right\}. \tag{6}$$

Given that the decision metric in (6) is a strictly increasing function of r_m, the decision rule in (6) can be broken down into two simpler rules as follows:

$$\hat{m} = \underset{m=1,\ldots,M}{\arg\max}\{r_m\}\ \ ;$$
$$\hat{p} = \underset{p=1,\ldots,P}{\arg\max}\left\{r_{\hat{m}}\log\left(1+\frac{I_p\lambda_s}{\lambda_b}\right)-I_p\lambda_s\right\}, \tag{7}$$

where the first rule indicates that, most probably, an optical signal has been transmitted in the slot having the maximum photo-electron count while the second rule solves for the specific transmit aperture that has been pulsed in this slot.

For OSSK, (7) simplifies to:

$$\hat{p} = \underset{p=1,\ldots,P}{\arg\max}\left\{r_1\log\left(1+\frac{I_p\lambda_s}{\lambda_b}\right)-I_p\lambda_s\right\}, \tag{8}$$

where r_1 stands for the number of photo-electrons collected over the entire symbol duration.

Assuming, without loss of generality, that the channel gains are sorted in an ascending order $I_1\leq\cdots\leq I_P$, then the decision rule in (8) is equivalent to:

$$\hat{p}=p\ \ \text{if}\ \ r_1\in[\gamma_p\ \ \gamma_{p+1}-1], \tag{9}$$

[2]For OSSK, there are no empty slots ($M-1=0$).

where, through direct calculations, it can be proven that the decision threshold between levels $p-1$ and p can be determined from:

$$\gamma_p = \left\lceil\frac{(I_p-I_{p-1})\lambda_s}{\log\left(\frac{I_p\lambda_s+\lambda_b}{I_{p-1}\lambda_s+\lambda_b}\right)}\right\rceil\ \ ;\ \ p=2,\ldots,P, \tag{10}$$

with $\gamma_1=0$ and $\gamma_{P+1}\to\infty$ while $\lceil x\rceil$ ceils x to the smallest integer larger than or equal to x.

Given that the parameters $\{I_p\}_{p=1}^{P}$, λ_s and λ_b do not depend on the transmitted OSM symbols, the implementation of the ML SPPM decoder in (7) requires carrying out $M+P$ comparisons, P multiplications and P additions per symbol duration. In this context, the values $\left\{\log\left(1+\frac{I_p\lambda_s}{\lambda_p}\right), I_p\lambda_s\right\}_{p=1}^{P}$ need to be calculated only once per fading block that extends over several thousands of symbol durations in the context of FSO communications. Consequently, the complexity associated with evaluating these $2P$ values can be neglected compared to the other operations that need to be carried out on a symbol-by-symbol basis. Similarly, the symbol-level operations associated with the ML OSSK decoder in (8) correspond to P comparisons, P multiplications and P additions. In this context, the advantage of the simplified ML OSSK decoding rule in (9) resides in requiring only P comparisons (with no time-consuming multiplication operations) since the threshold levels in (10) do not vary over a fading block duration.

III. Performance Analysis in the Open-Loop Scenario

In this section, we evaluate the performance of OSSK and SPPM in the open-loop scenario in the absence of channel state information (CSI) at the transmitter side. In this scenario, OSM will involve all P transmit apertures rather than a selection of these apertures.

A. Exact Symbol Error Probability (SEP)

1) OSSK: For OSSK, following from (9), a correct decision is made when the random variable R_1 falls between γ_p and $\gamma_{p+1}-1$ when the p-th transmit aperture is pulsed (i.e. $s_{p,1}=1$) for $p=1,\ldots,P$. Since, for $s_{p,1}=1$, R_1 is a Poisson random variable with parameter $I_p\lambda_s+\lambda_b$ from (3), and assuming all OSSK symbols to be equally likely, the conditional symbol error probability (SEP) of the OSSK scheme can be calculated as follows:

$$P_{e|\mathcal{I}}^{(\text{OSSK})} = 1-\frac{1}{P}\sum_{p=1}^{P}\sum_{k=\gamma_p}^{\gamma_{p+1}-1}\frac{e^{-(I_p\lambda_s+\lambda_b)}(I_p\lambda_s+\lambda_b)^k}{k!}, \tag{11}$$

where $\mathcal{I}\triangleq\{I_1,\ldots,I_P\}$ while the conditioning is performed over the P channel irradiances.

2) SPPM: For SPPM, following from (7), the wrong reconstruction of the slot index $\hat{m}$ will directly result in an OSM symbol error. Consequently, the conditional SEP of the SPPM scheme can be determined as follows:

$$P_{e|\mathcal{I}}^{(\text{SPPM})} = P_{e|\mathcal{I}}^{(\text{SPPM})}(\mathcal{S})+P_{e|\mathcal{I}}^{(\text{SPPM})}(\mathcal{A},\overline{\mathcal{S}}), \tag{12}$$

where $P_{e|\mathcal{I}}^{(\text{SPPM})}(\mathcal{S})$ stands for the probability of the event $\mathcal{S}$ corresponding to a slot index error. On the other hand, $P_{e|\mathcal{I}}^{(\text{SPPM})}(\mathcal{A},\overline{\mathcal{S}})$ stands for the probability of an aperture index error (event $\mathcal{A}$) when the slot index is reconstructed correctly ($\overline{\mathcal{S}}$ stands for the complement of the event $\mathcal{S}$).

The probability $P_{e|\mathcal{I}}^{(\text{SPPM})}(\mathcal{S})$ can be determined from:

$$P_{e|\mathcal{I}}^{(\text{SPPM})}(\mathcal{S}) = \frac{1}{MP}\sum_{p=1}^{P}\sum_{m=1}^{M}\Pr(\hat{m}\neq m|s_{p,m}=1) = \frac{1}{P}\sum_{p=1}^{P}\Pr(\hat{m}\neq 1|s_{p,1}=1), \quad (13)$$

where the second equality follows from the symmetry of the PPM constellation. Next, we derive the probability $\Pr(\hat{m}\neq 1|s_{p,1}=1) = 1-\Pr(\hat{m}=1|s_{p,1}=1)$. The relation $\hat{m}=1$ (when $s_{p,1}=1$) suggests that the maximum count is observed in slot-1 following from (7). However, the maximum count can be observed in other slots as well where, when this case arises, the best that the ML decoder can do is to break the tie randomly. In other words, when m slots, in addition to slot-1, contain the maximum count, the tie can be broken in favor of the correct slot-1 with probability $\frac{1}{m+1}$. Consequently:

$$\Pr(\hat{m}\neq 1|s_{p,1}=1) = 1-\sum_{m=0}^{M-1}\frac{1}{m+1}\times \sum_{\substack{\mathcal{C}\subset\{2,\ldots,M\}\\|\mathcal{C}|=m}}\prod_{i\in\mathcal{C}}\Pr(R_{\mathcal{C}_i}=R_1)\prod_{j\in\overline{\mathcal{C}}}\Pr(R_{\overline{\mathcal{C}}_j}<R_1), \quad (14)$$

where $\overline{\mathcal{C}}\triangleq\{2,\ldots,M\}\backslash\mathcal{C}$ while $\mathcal{C}_n$ stands for the n-th element of the set $\mathcal{C}$. Since $s_{p,1}=1$ implies that $R_2,\ldots,R_M$ are identically-distributed Poisson random variables with parameter λ_b following from (3), then(14) simplifies to:

$$\Pr(\hat{m}\neq 1|s_{p,1}=1) = 1-\sum_{m=0}^{M-1}\frac{1}{m+1}\times \binom{M-1}{m}\left[\Pr(R_{m'}=R_1)\right]^{m}\left[\Pr(R_{m''}<R_1)\right]^{M-1-m}, \quad (15)$$

where m' and m'' are integers in $\{2,\ldots,M\}$. Finally, expanding the probabilities in (15) and replacing in (13) results in:

$$P_{e|\mathcal{I}}^{(\text{SPPM})}(\mathcal{S}) = 1-\frac{1}{P}\sum_{p=1}^{P}\sum_{m=0}^{M-1}\frac{1}{m+1}\binom{M-1}{m}\times \sum_{k=0}^{+\infty}\frac{e^{-(I_p\lambda_s+\lambda_b)}(I_p\lambda_s+\lambda_b)^k}{k!}\times \left[\frac{e^{-\lambda_b}\lambda_b^k}{k!}\right]^{m}\left[\sum_{j=0}^{k-1}\frac{e^{-\lambda_b}\lambda_b^j}{j!}\right]^{M-1-m}. \quad (16)$$

On the other hand, $P_{e|\mathcal{I}}^{(\text{SPPM})}(\mathcal{A},\overline{\mathcal{S}}) = \left(1-P_{e|\mathcal{I}}^{(\text{SPPM})}(\mathcal{S})\right)P_{e|\mathcal{I}}^{(\text{SPPM})}(\mathcal{A}|\overline{\mathcal{S}})$ where the conditional probability $P_{e|\mathcal{I}}^{(\text{SPPM})}(\mathcal{A}|\overline{\mathcal{S}})$ can be determined as follows:

$$P_{e|\mathcal{I}}^{(\text{SPPM})}(\mathcal{A}|\overline{\mathcal{S}}) = \frac{1}{MP}\sum_{p=1}^{P}\sum_{m=1}^{M}\Pr(\hat{p}\neq p|\hat{m}=m,s_{p,m}=1) = \frac{1}{P}\sum_{p=1}^{P}\Pr(\hat{p}\neq p|\hat{m}=1,s_{p,1}=1), \quad (17)$$

where the second equality follows from the symmetry of the M slots. The conditions $\hat{m}=1$ and $s_{p,1}=1$ in (17) imply that the erroneous slots $2,\ldots,M-1$ are excluded from the decision process while R_1 is a Poisson random variable with parameter $I_p\lambda_s+\lambda_b$. Therefore, an error will occur if R_1 falls outside the interval $[\gamma_p\ \ \gamma_{p+1}-1]$ implying that $P_{e|\mathcal{I}}^{(\text{SPPM})}(\mathcal{A}|\overline{\mathcal{S}})$ is equal to the probability $P_{e|\mathcal{I}}^{(\text{OSSK})}$ in (11). Consequently:

$$P_{e|\mathcal{I}}^{(\text{SPPM})}(\mathcal{A},\overline{\mathcal{S}}) = \left(1-P_{e|\mathcal{I}}^{(\text{SPPM})}(\mathcal{S})\right)P_{e|\mathcal{I}}^{(\text{OSSK})}, \quad (18)$$

where $P_{e|\mathcal{I}}^{(\text{OSSK})}$ and $P_{e|\mathcal{I}}^{(\text{SPPM})}(\mathcal{S})$ are given in (11) and (16), respectively. Finally, the conditional SEP of SPPM is obtained by replacing (16) and (18) in (12).

B. Upper-Bounds on the Symbol Error Probability

While the expressions derived in (11) and (16) are useful in evaluating the conditional SEP in an exact manner, these expressions are complicated and, hence, fail in offering clear and intuitive insights on the performance of OSSK and SPPM systems. In particular, the aggregation of the derived conditional SEP expressions, for the sake of determining the SEPs, is very involved. Driven by the intractability of the exact analysis, this section tackles an approximate analysis that is useful in studying the asymptotic behavior of FSO-OSM systems.

Proposition *1:* The conditional probabilities in (11) and (16) can be upper-bounded as follows:

$$P_{e|\mathcal{I}}^{(\text{OSSK})} \leq \frac{1}{2P}\sum_{p=1}^{P}\sum_{\substack{p'=1\\p'\neq p}}^{P}e^{-\frac{1}{2}\left(\sqrt{I_p\lambda_s+\lambda_b}-\sqrt{I_{p'}\lambda_s+\lambda_b}\right)^2} \quad (19)$$

$$P_{e|\mathcal{I}}^{(\text{SPPM})}(\mathcal{S}) \leq \frac{M-1}{2P}\sum_{p=1}^{P}e^{-\left(\sqrt{I_p\lambda_s+\lambda_b}-\sqrt{\lambda_b}\right)^2}. \quad (20)$$

Proof: The proof is based on the Bhattacharyya bound [25], [26] and is provided in Appendix A. ■

Following from the fact that the channel irradiances $\{I_1,\ldots,I_P\}$ are identically-distributed, then the average SEPs can be derived from (19)-(20) as follows:

$$P_{e}^{(\text{OSSK})} \leq \frac{P-1}{2}\int_0^{+\infty}\int_0^{+\infty}e^{-\frac{1}{2}\left(\sqrt{\lambda_s x+\lambda_b}-\sqrt{\lambda_s y+\lambda_b}\right)^2}\times f_X(x)f_Y(y)\mathrm{d}x\mathrm{d}y \quad (21)$$

$$P_{e}^{(\text{SPPM})}(\mathcal{S}) \leq \frac{M-1}{2}\int_0^{+\infty}e^{-\left(\sqrt{\lambda_s x+\lambda_b}-\sqrt{\lambda_b}\right)^2}f_X(x)\mathrm{d}x, \quad (22)$$

where the gamma-gamma pdf $f_I(I)$ is given in (1).

C. Asymptotic Analysis and Diversity Order

In this section, we carry out an asymptotic analysis that is useful for deriving the transmit diversity order of open-loop FSO-OSM systems under gamma-gamma scintillation.

Proposition *2:* For $\lambda_s \gg \lambda_b$, the average SEP in (21) behaves asymptotically as $\lambda_s^{-\frac{1}{2}}$ implying a transmit diversity order of $1/2$.

Proof: The proof is based on approximating the gamma-gamma distribution by the versatile mixture gamma distribution over the entire range of irradiances [27], [28]. This proof is provided in Appendix B. ∎

Proposition *3:* For $\lambda_s \gg \lambda_b$, the average SEP in (22) behaves asymptotically as $\lambda_s^{-\beta}$ implying a transmit diversity order of β.

Proof: The proof is based on performing the power series expansion of the gamma-gamma pdf near the origin [29]. This proof is provided in Appendix C. ∎

The reason for adopting the mixture gamma distribution and the series expansion for proving proposition 2 and proposition 3, respectively, is as follows. The SEP in (21) is dominated by small values of $\sqrt{\lambda_s x + \lambda_b} - \sqrt{\lambda_s y + \lambda_b}$. This quantity can be small even if x and y are large necessitating an approximation to the gamma-gamma pdf that holds for all values of the irradiance. This makes the mixture gamma distribution an appropriate option for evaluating the diversity order. On the other hand, the integral in (22) is dominated exclusively by small values of x rendering the simpler approach of performing a power series expansion near the origin sufficient for evaluating the asymptotic behavior of the SEP.

D. Analysis and Conclusions

From proposition 2, the transmit diversity order of the open-loop OSSK scheme is $\delta^{(\text{OSSK})} = \frac{1}{2}$. On the other hand, from (12) and (18),:

$$P_e^{(\text{SPPM})} = P_e^{(\text{SPPM})}(\mathcal{S}) + \left(1 - P_e^{(\text{SPPM})}(\mathcal{S})\right) P_e^{(\text{OSSK})} \quad (23)$$

$$\approx P_e^{(\text{SPPM})}(\mathcal{S}) + P_e^{(\text{OSSK})}, \quad (24)$$

where the approximation holds for large values of λ_s.

Therefore, following from proposition 2 and proposition 3, the transmit diversity order of the open-loop SPPM scheme is given by $\delta^{(\text{SPPM})} = \min\left\{\beta, \frac{1}{2}\right\}$. A simple numerical analysis shows that $\beta \geq 1$ for different link distances (d) and for different values of the refractive index structure parameter C_n^2 resulting in:

$$\delta^{(\text{OSSK})} = \delta^{(\text{SPPM})} = \frac{1}{2} \;\; ; \;\; \forall\, d \;,\; \forall\, C_n^2 \;,\; \forall\, P, \quad (25)$$

since proposition 2 shows that the diversity order of $P_e^{(\text{OSSK})}$ does not depend on P.

Therefore, the following conclusions regarding the open-loop scenario can be drawn:

- Equation (25) shows that the diversity orders of OSSK and SPPM do not depend neither on the channel parameters nor on the number of transmit apertures P. This result, obtained under the Poisson model, is coherent with the previously reported results in the context of RF-SM [3], [4] and FSO-OSM [15]–[17] systems under the AWGN model. Moreover, the value of $1/2$ is in coherence with [15]–[17]. This result can be interpreted as follows. For both schemes, the error performance is dominated by the aperture index errors (with probability $P_e^{(\text{OSSK})}$). This type of errors is related to the receiver's capability of distinguishing between the P channel irradiances and, consequently, is small (resp. large) when the channel gains assume remarkably different (resp. comparable) values. Now, as the link distance increases, the P identically-distributed channel gains will all decrease on average (and vice versa) implying that all of the channel gains will move in the same direction, thus not affecting the receiver's ability to differentiate between the channel gains. This is better clarified in (19) that shows that the SEP involves the quantity $\sqrt{I_p} - \sqrt{I_{p'}}$ (for $\lambda_b \ll 1$) where this quantity is small if the values I_p and $I_{p'}$ are close to each other (even if they are both large). On the other hand, the slot index error probability in (20) depends on I_p implying that increasing I_p (by decreasing the link distance) will reduce this type of error.
- The diversity orders achieved by the two considered open-loop OSM schemes are the same.
- For average-to-large values of λ_s, the slot index errors can be neglected compared to the aperture index errors.
- The diversity order of the OSM schemes is smaller than the diversity order of SISO systems (that is equal to β). Therefore, unlike RF-SM systems (with Rayleigh fading) where the extension from the SISO to the MISO scenarios involves an increase in the bit rate with no reduction in the transmit diversity order [3], [4], the extension of SISO-FSO systems to MISO-FSO systems incurs a reduction in the transmit diversity order.

E. Numerical Validation

Next, we present some numerical results that validate the conclusions of the previous section. The numerical results are obtained through Monte Carlo simulations over a total of 10^4 channel realizations. A block fading model was considered with each block extending over 10^3 symbol durations where the channel irradiances vary independently from one block to another. For each block, after generating the P-ary (resp. MP-ary) uniform OSSK (resp. SPPM) symbols, the P channel iradiances are generated according to the pdf in (1). At a second stage, the Poisson-distribued decision variables are generated according to (3). Finally, the ML decison rule in (7) is applied and the reconstructed symbols are compared with the information symbols for the sake of determining the SEP. The theoretical results were generated based on equations (11), (12), (16) and (18). In this context, truncating the summation in (16) at 10^5 terms is sufficient for generating accurate results over the entire considered range of values of E_s.

The performance of SPPM for a link distance of 3 km is shown in Fig. 2 and Fig. 3 where we set $(P, M) = (4, 4)$ and $(P, M) = (8, 8)$, respectively. This way, each OSM symbol encompasses 4 bits and 6 bits, respectively. The error rates

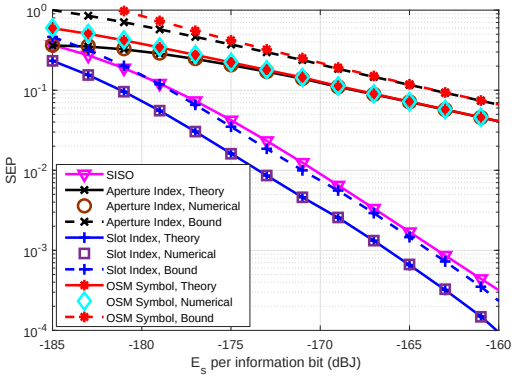

Fig. 2. Performance of SPPM with $P = 4$ and $M = 4$ for a link distance of 3 km. The error rates of the aperture index $P_e^{(\text{SPPM})}(\mathcal{A}, \overline{\mathcal{S}})$, slot index $P_e^{(\text{SPPM})}(\mathcal{S})$ and OSM symbol $P_e^{(\text{SPPM})}$ are shown. The theoretical results are obtained by numerically aggregating the conditional SEPs in (11) and (16) while the bounds are given in (21) and (22).

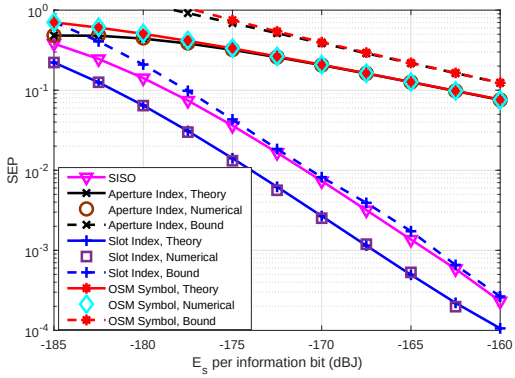

Fig. 3. Performance of SPPM with $P = 8$ and $M = 8$ for a link distance of 3 km. The error rates of the aperture index $P_e^{(\text{SPPM})}(\mathcal{A}, \overline{\mathcal{S}})$, slot index $P_e^{(\text{SPPM})}(\mathcal{S})$ and OSM symbol $P_e^{(\text{SPPM})}$ are shown. The theoretical results are obtained by numerically aggregating the conditional SEPs in (11) and (16) while the bounds are given in (21) and (22).

of the aperture index $P_e^{(\text{SPPM})}(\mathcal{A}, \overline{\mathcal{S}})$, slot index $P_e^{(\text{SPPM})}(\mathcal{S})$ and OSM symbol $P_e^{(\text{SPPM})}$ are explicitly shown in Fig. 2 and Fig. 3. Results show the extremely close match between the theoretical and numerical results thus highlighting on the accuracy of the SEP expressions derived in Section III-A. Results in Fig. 2 and Fig. 3 also highlight on the usefulness of the bounds provided in (21)-(22) for predicting the error performance for average-to-large values of the signal energy E_s. In particular, the proposed upper-bounds have the same slopes as the exact SEPs since the corresponding curves are practically parallel to each other for large values of E_s. This shows that the proposed bounds are particularly convenient for determining the diversity orders of the OSSK and SPPM schemes. Results also validate proposition 2, proposition 3 and (25) where $P_e^{(\text{SPPM})}(\mathcal{S})$ has a diversity order of β (that is equal to 1.53 in this scenario) while $P_e^{(\text{SPPM})}(\mathcal{A}, \overline{\mathcal{S}})$ and $P_e^{(\text{SPPM})}$ have a diversity order of $1/2$. In this context, the OSM performance is dominated by $P_e^{(\text{SPPM})}(\mathcal{A}, \overline{\mathcal{S}})$ and results in Fig. 2 and Fig. 3 show that $P_e^{(\text{SPPM})} \approx P_e^{(\text{SPPM})}(\mathcal{A}, \overline{\mathcal{S}})$ for the values of $\frac{E_s}{\log_2(MP)}$ exceeding -175 dBJ. Finally, results underscore the significant performance gap between SISO and OSM systems where the additional $\log_2(P)$ bits encoded in the index of the pulsed transmit aperture incur high SEP degradations especially for large value of E_s.

Fig. 4 shows the impact of the turbulence strength on the performance of open-loop OSSK and SPPM (with $M = 4$) systems for a link distance of 3 km. In particular, we compare the strong turbulence and weak-to-average turbulence scenarios with $C_n^2 = 10^{-12}$ m$^{-2/3}$ and $C_n^2 = 5 \times 10^{-16}$ m$^{-2/3}$, respectively. Results validate the finding in (25) where the diversity order is equal to $1/2$ regardless of the values of C_n^2 and P. Moreover, for both OSSK and SPPM, the SEP increases with P where the achieved multiplexing gains are associated with performance losses. Results in Fig. 4 highlight the central finding that OSM systems are more suitable for severe turbulence conditions where the SEP is smaller under strong turbulence. This behavior, that contradicts the conventional behavior of single-aperture systems, is justified by the fact that the Rytov variance increases with C_n^2. Therefore, the variability of the P channel irradiances is higher under strong turbulence implying that the OSM receiver will have better chances for accurately predicting the index of the pulsed aperture. For example, under the extreme hypothetical assumption of zero variability (no turbulence), the P identically-distributed channel irradiances will be the same implying that the receiver will not be able to recognize which transmit aperture was pulsed.

Results in Fig. 4 also show that SPPM performs better than OSSK where the additional $\log_2(M)$ bits transmitted by SPPM are associated with an appealing improvement in the SEP. In this context, the interest of OSSK resides in its remarked simplicity rendering this simple solution an appealing alternative to SPPM. Finally, it is worth highlighting that the need to study OSSK stems from the fact that deriving the SEP of SPPM ($P_e^{(\text{SPPM})}$) requires the derivation of the SEP of OSSK ($P_e^{(\text{OSSK})}$) since $P_e^{(\text{SPPM})}$ is related to $P_e^{(\text{OSSK})}$ according to (23).

IV. Performance Analysis in the Closed-Loop Scenario

A. Preliminaries

In this section, we analyze closed-loop OSM systems where partial CSI is assumed to be available at the transmitter side. In this scenario, we prove that combined multiplexing gains and diversity gains can be achieved and we propose a transmit aperture selection scheme that maximizes the achievable diversity order for a target data rate.

The transmit aperture selection scheme revolves around limiting the transmission to P_s transmit apertures out of the P available apertures with $P_s \leq P$. This selection reduces the data rate to $\log_2(MP_s)$ bpcu (with M indicating the number of PPM positions for SPPM while $M = 1$ for OSSK). In general, P_s is taken to be a power of two so that $\log_2(MP_s)$ is an integer (in general M is a power of two as well for M-ary PPM constellations). This way, each one of the MP_s OSM symbols can be mapped into a sequence of $\log_2(MP_s)$ bits. The selection scheme will be based on the

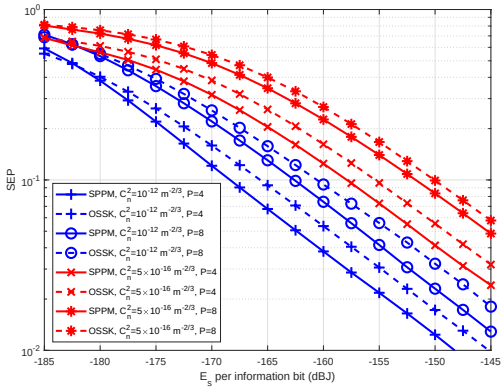

Fig. 4. Performance of OSSK and SPPM (with $M = 4$) with $P = 4$ and $P = 8$ for a link distance of 3 km under different turbulence conditions.

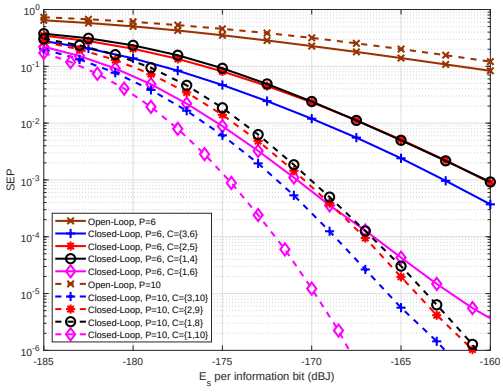

Fig. 5. Performance of OSSK with $P_s = 2$ selected transmit apertures for a link distance of 3 km.

values of the P channel irradiances that, without any loss of generality, are assumed to be arranged in an increasing order: $I_1 \leq I_2 \leq \cdots \leq I_P$.

The proposed selection scheme does not entail the knowledge of the exact values of the path gains $\{I_1, \ldots, I_P\}$ at the transmitter side where this full-CSI availability is not practical. Contrariwise, only the indices of the P_s selected apertures are fed back from the receiver to the transmitter where this selection is carried out at the receiver based simply on sorting the P channel irradiances. In this context, a quantized feedback link of P bits is sufficient for the considered aperture selection scheme where, for example, the p-th transmit aperture will be included (resp. not included) in the pool of selected apertures if the p-th feedback bit is equal to 1 (resp. 0). Given the very large coherence time of FSO channels, this limited feedback of P bits is not resource-consuming since these bits need to be communicated to the transmitter only once per fading block that extends over thousands of symbol durations.

In what follows, we assume that the selection scheme limits the transmission to the apertures whose indices belong to the set $\mathcal{C}$ where $\mathcal{C} \subset \{1, \ldots, P\}$ with $|\mathcal{C}| = P_s$.

B. Asymptotic Analysis and Diversity Order

Since the conditional probability in (19) does not change if the values of I_p and $I_{p'}$ are interchanged, the corresponding average error probability can be written as:

$$P_{e|\mathcal{I}}^{(\mathrm{OSSK})} = \frac{1}{P} \sum_{p \in \mathcal{C}} \sum_{\substack{p' \in \mathcal{C} \\ p' > p}} \int_0^{+\infty} \int_0^{y} e^{-\frac{1}{2}\left(\sqrt{\lambda_s y + \lambda_b} - \sqrt{\lambda_s x + \lambda_b}\right)^2} f_{I_p, I_{p'}}(x, y) \mathrm{d}x \mathrm{d}y, \quad (26)$$

where $f_{I_p, I_{p'}}(x, y)$ (with $0 \leq x \leq y$) stands for the joint pdf of the ordered random variables I_p and $I_{p'}$ (with $I_p \leq I_{p'}$) where this expression can be obtained based on order statistics [30, 2.3.2].

Similarly, integrating (20) results in:

$$P_{e|\mathcal{I}}^{(\mathrm{SPPM})}(\mathcal{S}) = \frac{M-1}{2P} \sum_{p \in \mathcal{C}} \int_0^{+\infty} e^{-\left(\sqrt{\lambda_s x + \lambda_b} - \sqrt{\lambda_b}\right)^2} f_{I_p}(x) \mathrm{d}x, \quad (27)$$

where $f_{I_p}(x)$ ($x \geq 0$) stands for the pdf of the p-th order statistic given in [30, 2.2.2].

Proposition *4:* For $\lambda_s \gg \lambda_b$, the integral in (26) behaves asymptotically as $\lambda_s^{-\frac{p'-p}{2}}$ implying a transmit diversity order of $\frac{p'-p}{2}$ (where $p \leq p'$).

Proof: The proof is based on approximating the gamma-gamma distribution by the mixture gamma distribution [27], [28]. This proof is provided in Appendix D. ■

Proposition *5:* For $\lambda_s \gg \lambda_b$, the integral in (27) behaves asymptotically as $\lambda_s^{-p\beta}$ implying a transmit diversity order of $p\beta$.

Proof: The proof is based on the power series expansion of the gamma-gamma pdf [29]. This proof is provided in Appendix E. ■

Proposition 4 and proposition 5 imply the following expressions for the optimal transmit diversity orders that can be achieved when aperture selection is associated with the closed-loop OSSK and SPPM schemes:

$$\delta^{(\mathrm{OSSK})} = \max_{\substack{\mathcal{C} \subset \{1, \ldots, P\} \\ |\mathcal{C}| = P_s}} \left\{ \min_{\substack{p, p' \in \mathcal{C} \\ p < p'}} \frac{\mathcal{C}_{p'} - \mathcal{C}_p}{2} \right\};$$

$$\delta^{(\mathrm{SPPM})} = \max_{\substack{\mathcal{C} \subset \{1, \ldots, P\} \\ |\mathcal{C}| = P_s}} \left\{ \min \left\{ \min\{\mathcal{C}\}\beta, \min_{\substack{p, p' \in \mathcal{C} \\ p < p'}} \frac{\mathcal{C}_{p'} - \mathcal{C}_p}{2} \right\} \right\}, \quad (28)$$

where $\mathcal{C}_p$ stands for the p-th element of the set $\mathcal{C}$. Equation (28) shows that, as in the open-loop scenario with no aperture selection, the diversity order of the OSSK scheme does not depend on the properties of the underlying FSO channel in the closed-loop scenario as well.

Finally, it is worth noting that when all transmit apertures are selected, $\mathcal{C} = \{1, \ldots, P\}$ implying that the diversity orders in (28) will simplify to $\delta^{(\mathrm{OSSK})} = \frac{1}{2}$ and $\delta^{(\mathrm{SPPM})} = \min\{\beta, \frac{1}{2}\} = \frac{1}{2}$ which correspond to the values obtained in (25) in the open-loop scenario.

In order to validate proposition 4 and (28), Fig. 5 shows the impact of the selected aperture set $\mathcal{C}$ on the performance for the case $P_s = 2$. Simulations are performed with OSSK for a link distance of 3 km. For comparison purposes, the performance of open-loop systems is shown as well. Following from (28),

the diversity order for a given set $\mathcal{C}$ when $P_s = 2$ is equal to $\frac{\max\{\mathcal{C}\}-\min\{\mathcal{C}\}}{2}$. Consequently, we compare the suboptimal sets $\{3, P\}$, $\{2, P-1\}$ and $\{1, P-2\}$ that all result in the same diversity order of $\frac{P-3}{2}$ where the comparison is carried out for the two cases of $P = 6$ and $P = 10$. We also show the performance with the set $\{1, P\}$ that achieves the highest diversity order of $\frac{P-1}{2}$ when $P_s = 2$. Results in Fig. 5 validate all of the previous findings where the SEP curves corresponding to the sets $\{3, 6\}$, $\{2, 5\}$ and $\{1, 4\}$ (when $P = 6$) are practically parallel to each other for large values of E_s and where the obtained diversity order is confirmed to be $3/2$. In this scenario, the set $\{1, 6\}$ increases the diversity order to $5/2$ which is validated in Fig. 5 where the associated SEP curve is steeper. This results in significant performance gains especially for large values of E_s. For example, comparing the sets $\{1, 6\}$ and $\{3, 6\}$ shows that the former selection outperforms the latter one by 8.5 dB at a SEP of 10^{-3}. The same holds for the case $P = 10$ where the three considered sets $\{3, 10\}$, $\{2, 9\}$ and $\{1, 8\}$ result in the same diversity order that is increased to the value of $7/2$. In fact, the corresponding SEP curves are parallel to each other for large values of E_s and the diversity order of $7/2$ is validated numerically. In this case, increasing the number of transmit apertures from 6 to 10 enhances the diversity order by a factor of $7/3$ while transmitting at the same rate of 1 bpcu. Finally, unlike open-loop systems where the performance deteriorates when P increases, the SEP of closed-loop systems decreases with P. This is justified by the fact that the diversity order in (28) increases with P for a fixed value of P_s. In this case, as in space-time coded systems, increasing the value of P contributes to increasing the diversity order.

In coherence with (28), the same values of the diversity order were obtained for other values of the link distance but the results are not presented here for the sake of brevity. The justification is similar to the one presented in Section III-D. Results in Fig. 5 also show that, among the three considered suboptimal sets, the set $\{3, P\}$ results in the highest coding gain. In fact, $I_P \geq I_{P-1} \geq I_{P-2}$ while $I_3 \geq I_2 \geq I_1$ implying that the transmission takes place along two channels that have stronger irradiances compared to the channels of the two other suboptimal options. Finally, results show the huge performance gap between the suboptimal selection strategies and the set $\{1, P\}$ that achieves the highest diversity gain. For example, at a SEP of 10^{-3}, pulsing one of the apertures 1 or P rather than pulsing one of the apertures 3 or P results in performance gains in the order of 8.2 dB and 2.6 dB for $P = 6$ and $P = 10$, respectively. Evidently, this performance gap will increase for smaller values of the SEP.

C. Proposed Aperture Selection Scheme and Conclusions

In this section, we solve for the set $\mathcal{C}$ that maximizes the diversity order in (28) for OSSK and SPPM. Denoting by p the smallest integer in $\mathcal{C}$, (28) can be written as:

$$\delta^{(\text{OSSK})} = \max_{p=1,\ldots,P} \left\{ \frac{1}{2} \left\lfloor \frac{P-p}{P_s-1} \right\rfloor \right\} \; ;$$
$$\delta^{(\text{SPPM})} = \max_{p=1,\ldots,P} \left\{ p\beta, \frac{1}{2} \left\lfloor \frac{P-p}{P_s-1} \right\rfloor \right\}. \quad (29)$$

In fact, the quantity $\min_{\substack{p,p' \in \mathcal{C} \\ p<p'}} (\mathcal{C}_{p'} - \mathcal{C}_p)$ is maximized if the aperture indices are selected to be uniformly spaced along the interval $[\min\{\mathcal{C}\} \; \max\{\mathcal{C}\}] = [p \; \max\{\mathcal{C}\}]$. This separation is further maximized if $\max\{\mathcal{C}\}$ is selected to be equal to P. Now, if the smallest aperture index is selected to be p and the largest aperture index is selected to be P, then selecting the $P_s - 2$ remaining indices (i.e. the remaining elements of $\mathcal{C}$) equidistantly between p and P results in the maximum possible separation of $\left\lfloor \frac{P-p}{(P_s-2)+1} \right\rfloor = \left\lfloor \frac{P-p}{P_s-1} \right\rfloor$ that appears in the expression of $\delta^{(\text{OSSK})}$ in (29). Therefore, it follows directly that:

$$\delta^{(\text{OSSK})} = \frac{1}{2} k_{\text{opt}} \quad ; \quad k_{\text{opt}} \triangleq \left\lfloor \frac{P-1}{P_s-1} \right\rfloor, \quad (30)$$

if the set $\mathcal{C}$ is selected as:

$$\mathcal{C} = \{P - k_{\text{opt}}(P_s-1), P - k_{\text{opt}}(P_s-2), \ldots, P\}, \quad (31)$$

where this choice of $\mathcal{C}$ results in the maximum possible separation of k_{opt} between any two consecutive elements of $\mathcal{C}$ implying a maximum diversity order of $\frac{1}{2}k_{\text{opt}}$.

It is worth noting that other choices of the selected set under the form $\mathcal{C}' = \{x - p' \; ; \; x \in \mathcal{C}\}$ will result in the same separation of k_{opt} (and in the same diversity order of $\frac{1}{2}k_{\text{opt}}$) where p' is any integer such that $\min\{C\} - p' \geq 1$. However, unlike $\mathcal{C}'$, the set $\mathcal{C}$ encompasses the apertures with the highest channel irradiances resulting in an enhanced coding gain based on the findings drawn from Fig. 5. For example, for $P = 9$ and $P_s = 4$, $k_{\text{opt}} = 2$ implying that $\mathcal{C} = \{3, 5, 7, 9\}$ from (31) where this set results in the maximum achievable diversity order of 1 following from (30). Now, the other options $\mathcal{C}' = \{2, 4, 6, 8\}$ and $\mathcal{C}' = \{1, 3, 5, 7\}$ will result in the same value of the diversity order; however, $\mathcal{C}_i > \mathcal{C}'_i$ for $i = 1, \ldots, 4$ implying that the set $\mathcal{C}$ will result in higher coding gains since the involved path gains are stronger.

Finally, it is worth noting that with no aperture selection ($P_s = P$), (30) and (31) imply that $k_{\text{opt}} = 1$, $\delta^{(\text{OSSK})} = \frac{1}{2}$ and $\mathcal{C} = \{1, \ldots, P\}$ where this value of $\mathcal{C}$ is expected while the achievable transmit diversity order is coherent with (25).

Similar to the analysis presented in the case of OSSK, the following proposition holds for SPPM.

Proposition *6:* For closed-loop SPPM, the highest transmit diversity order that can be achieved when P_s apertures are selected out of P apertures is given by:

$$\delta^{(\text{SPPM})} \triangleq \max \left\{ \delta_1^{(\text{SPPM})}, \delta_2^{(\text{SPPM})} \right\}$$
$$= \max \left\{ \frac{1}{2}\tilde{k}, [P - (\tilde{k}+1)(P_s-1)]\beta \right\}, \quad (32)$$

where:

$$\tilde{k} = \left\lfloor \frac{2P\beta}{1 + 2(P_s-1)\beta} \right\rfloor. \quad (33)$$

This maximum diversity order is achieved if the set $\mathcal{C}$ is selected as:

$$\mathcal{C} = \{P - k_{\text{opt}}(P_s-1), P - k_{\text{opt}}(P_s-2), \ldots, P\}, \quad (34)$$

where:

$$k_{\text{opt}} = \begin{cases} \tilde{k}, & \delta_1^{(\text{SPPM})} \geq \delta_2^{(\text{SPPM})}; \\ \tilde{k}+1, & \delta_1^{(\text{SPPM})} < \delta_2^{(\text{SPPM})}. \end{cases} \quad (35)$$

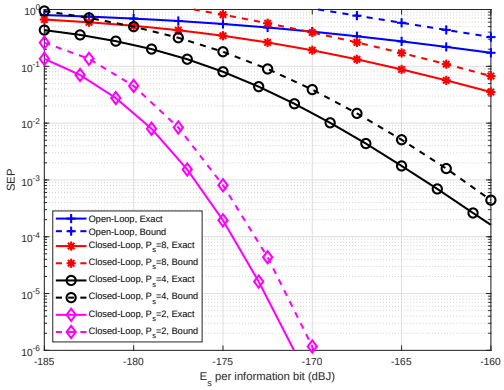

Fig. 6. The impact of the number of selected apertures (P_s) on the performance of OSSK with 16 transmit apertures for a link distance of 3 km.

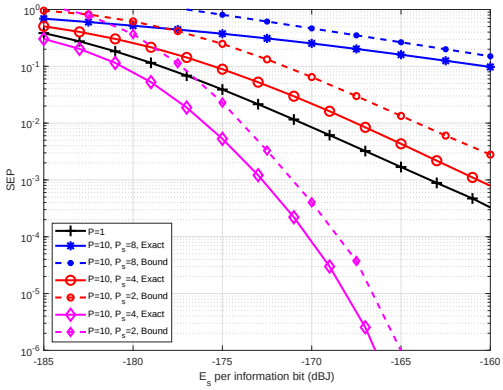

Fig. 7. The impact of the number of selected apertures (P_s) on the performance of SPPM with 10 transmit apertures and 8-PPM for a link distance of 3.2 km.

Proof: The proof is provided in Appendix F. ■

Consider the special case $P_s = P$. If $\beta < \frac{1}{2}$, then $\tilde{k} = 0$ and $(\delta_1^{(\text{SPPM})}, \delta_2^{(\text{SPPM})}) = (0, \beta)$ implying that $\delta^{(\text{SPPM})} = \beta$ and $k_{\text{opt}} = 1$. If $\beta \geq \frac{1}{2}$, then $\tilde{k} = 1$ and $(\delta_1^{(\text{SPPM})}, \delta_2^{(\text{SPPM})}) = (\frac{1}{2}, (2-P)\beta)$ implying that $\delta^{(\text{SPPM})} = \frac{1}{2}$ and $k_{\text{opt}} = 1$. Therefore, $\delta^{(\text{SPPM})} = \min\{\frac{1}{2}, \beta\}$ in coherence with the results in Section III-D. Finally, $k_{\text{opt}} = 1 \Rightarrow \mathcal{C} = \{1, \ldots, P\}$.

Based on the above analysis, the following conclusions can be drawn:

- Equations (30) and (32) show that, unlike the case of open-loop systems, the closed-loop FSO-OSM solutions are capable of increasing both the bit rate and diversity order with respect to single-aperture systems. The smaller P_s is compared to P, the higher the diversity gain that can be reaped from the FSO-OSM solutions.
- As in the case of open-loop systems, the diversity order achieved by closed-loop OSSK does not depend on the channel parameters and severity of scintillation.
- The last observation does not hold for closed-loop SPPM. In fact, from (32), depending on the values of P, P_s and β, the channel-independent quantity $\delta_1^{(\text{SPPM})}$ might be smaller or larger than the channel-dependent quantity $\delta_2^{(\text{SPPM})}$.
- For both OSSK and SPPM, increasing the value of P_s increases the bit rate at the expense of decreasing the diversity gain until it reaches the minimum value of $\frac{1}{2}$ when $P_s = P$.

It is worth noting that the presented performance analysis and aperture selection scheme can be readily extended to $P \times Q$ MIMO systems with $Q > 1$ in the case where equal gain combining (EGC) is applied at the receiver. For this suboptimal detection scheme, all of the previously presented derivations hold where the channel irradiances $\{I_p\}_{p=1}^{P}$ and noise parameter λ_b need to be simply replaced by $\{\sum_{q=1}^{Q} I_{p,q}\}_{p=1}^{P}$ and $Q\lambda_b$, respectively, where $I_{p,q}$ stands for the channel irradiance between the p-th laser and q-th photo-detector. However, with ML detection, the decision rule can not be decoupled as in (7) thus significantly altering the associated SEP analysis. While this paper initiated the investigation of OSM MISO techniques with photon-counting receivers, future research can build on this work for tackling the more general MIMO case.

D. Numerical Validation

Fig. 6 shows the impact of aperture selection with OSSK for $P = 16$ and a link distance of 3 km. The scenarios $P_s = 2, 4, 8$ are considered achieving the diversity orders of $15/2$, $5/2$ and 1 at the data rates of 1 bpcu, 2 bpcu and 3 bpcu, respectively. The selected apertures are based on (31) that results in $\mathcal{C} = \{1, 16\}$, $\mathcal{C} = \{1, 6, 11, 16\}$ and $\mathcal{C} = \{2, 4, 6, 8, 10, 12, 14, 16\}$ for the values of P_s equal to 2, 4 and 8, respectively. We also compare the closed-loop systems with the open-loop system that achieves a diversity order of $1/2$ while transmitting at the rate of 4 bpcu. The results in Fig. 6 validate the diversity orders given in (30). As indicated above, increasing P_s increases the data rate at the expense of reducing the diversity order and hence the SEP performance. Comparing the cases $P_s = 2$ and $P_s = 4$, transmitting one additional bpcu incurs a performance loss of about 10 dB at a SEP of 10^{-3}. In practice, P_s must be selected to be neither very large nor very small resulting in an acceptable level of compromise between the data and error rates. In this context, comparing the closed-loop and open-loop scenarios shows that the latter case results in the highest data rate and smallest diversity order. Results in Fig. 6 also highlight on the huge SEP gap between open-loop and closed-loop systems having small values of P_s. Finally, as in the open-loop case, results in Fig. 6 validate the accuracy of the proposed upper-bounds in predicting the diversity order of closed-loop systems as well.

Fig. 7 shows the impact of aperture selection with SPPM for $P = 10$, $M = 8$ and a link distance of 3.2 km. The scenarios $P_s = 2, 4, 8$ are considered resulting in the data rates of 4 bpcu, 5 bpcu and 6 bpcu, respectively. As a benchmark, we also show the performance of the 8-PPM SISO system that transmits at the rate of 3 bpcu. For the considered link distance, $\beta = 1.46$ implying that the diversity order of the SISO system is equal to 1.46. From (32)-(33), for $P_s = 2$, $\delta_1^{(\text{SPPM})} = 3.5 \geq \delta_2^{(\text{SPPM})} = 2\beta = 2.92$ and, for $P_s = 8$, $\delta_1^{(\text{SPPM})} = 0.5 \geq \delta_2^{(\text{SPPM})} = -4\beta = -5.84$.

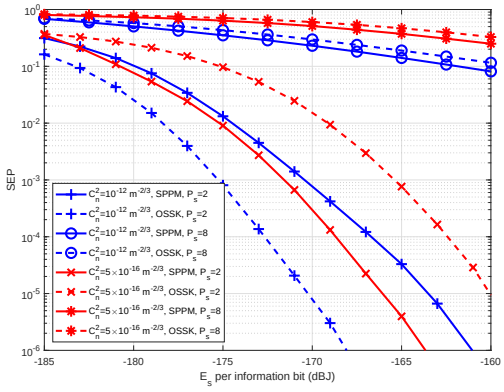

Fig. 8. Performance of OSSK and SPPM (with $M = 8$) with $P = 12$ for a link distance of 3 km under different turbulence conditions.

From (34)-(35), this implies that $k_{\text{opt}} = \tilde{k}$ that is equal to 7 ($\mathcal{C} = \{3, 10\}$) and 1 ($\mathcal{C} = \{3, \ldots, 10\}$) for $P_s = 2$ and $P_s = 8$, respectively. The opposite relation holds for $P_s = 4$ where $\delta_1^{(\text{SPPM})} = 1 < \delta_2^{(\text{SPPM})} = \beta = 1.46$ implying that $k_{\text{opt}} = \tilde{k} + 1 = 3$ resulting in $\mathcal{C} = \{1, 4, 7, 10\}$. Therefore, the achievable diversity orders are equal to 3.5, 1.46 and 0.5 for the values of P_s equal to 2, 4 and 8, respectively. This analysis shows that, unlike open-loop systems, the parameter β has an impact on the achievable diversity orders with closed-loop SPPM. In this case, the SPPM scheme with $P_s = 4$ profits from the same diversity order of the SISO system while transmitting 2 additional bpcu. This achievable diversity order is validated in Fig. 7 where the corresponding SEP curves are practically parallel to each other for large values of E_s. Results also show that this enhanced transmission rate is associated with a performance loss in the order of 3 dB. Finally, as in the case of OSSK, the scenario $P_s = 2$ results in the best performance. This scheme transmits one additional bpcu compared to SISO systems while profiting from a diversity gain that is 2.18 times higher resulting in a performance gain of about 9.5 dB at a SEP of 10^{-3}.

Fig. 8 compares the performance of closed-loop systems with OSSK and SPPM (with $M = 8$) under different turbulence conditions. We consider a link distance of 3 km with $P = 12$ and $P_s \in \{2, 8\}$. We also compare the scenarios of strong turbulence ($C_n^2 = 10^{-12}$ m$^{-2/3}$) and weak-to-average turbulence ($C_n^2 = 5 \times 10^{-16}$ m$^{-2/3}$). As in the open-loop scenario in Fig. 4, results in Fig. 8 highlight on the suitability of OSM to the strong turbulence conditions in the closed-loop scenario as well. For $P_s = 8$, results in Fig. 8 highlight that OSSK and SPPM achieve the same diversity order of $1/2$ for the two considered values of C_n^2 in coherence with (30) and (32). For this large value of P_s that privileges higher multiplexing gains at the expense of reduced diversity gains, SPPM manifests better performance compared to OSSK in analogy with the findings in the open-loop scenario in Fig. 4. For $P_s = 2$, SPPM maintains its superiority under weak-to-average turbulence where the diversity orders of both SPPM and OSSK are equal to 5.5. However, under strong turbulence, OSSK maintains the same diversity order of 5.5 (since the diversity order of OSSK depends only on P and P_s from (30)) while the diversity order of SPPM drops to 4 (in coherence with (32)). This reduction in the SPPM diversity order is reflected by the superiority of OSSK compared to SPPM under strong turbulence for $P_s = 2$.

V. Conclusion

OSM constitutes a viable option for FSO IM/DD communications under weather turbulence. An error probability analysis demonstrated that the diversity order does not depend on the severity of scintillation in the open-loop scenario. Moreover, significant diversity gains can be reaped from the proposed transmit aperture selection scheme in the closed-loop scenario. In this case, a tradeoff exists between the achievable multiplexing gains and diversity gains thus offering a leeway in the design of practical multi-aperture FSO systems. Two OSM schemes, namely OSSK and SPPM, were advised and contrasted under different turbulence conditions. While SPPM always manifests better performance in the open-loop scenario, the superiority of one of the two schemes depends on the turbulence conditions and number of activated apertures in the closed-loop scenario. Future research directions include the extension of this work to the case where the receiver is equipped with more than one aperture.

Appendix A

The aperture index error in (11) can be upper-bounded as follows:

$$P_{e|\mathcal{I}}^{(\text{OSSK})} \leq \frac{1}{P} \sum_{p=1}^{P} \sum_{\substack{p'=1 \\ p' \neq p}}^{P} \Pr(s_{p,1} \to s_{p',1}), \tag{36}$$

where $\Pr(s_{p,1} \to s_{p',1})$ is the pairwise error probability of pulsing aperture p (i.e. $s_{p,1} = 1$) and deciding in favor of aperture $p' \neq p$ (i.e. $s_{p',1} = 1$). Based on the Bhattacharyya bound, this pairwise error probability can be bounded as follows [25], [26]:

$$\Pr(s_{p,1} \to s_{p',1}) \leq \frac{1}{2} \sum_{r=0}^{+\infty} \sqrt{\Pr(R_1 = r | s_{p,1} = 1) \Pr(R_1 = r | s_{p',1} = 1)}, \tag{37}$$

where the factor $1/2$ follows from the improvement proposed in [26]. Following from the Poisson statistics whose parameters are given in (3), equation (37) can be written as:

$$\begin{aligned} &\Pr(s_{p,1} \to s_{p',1}) \\ &\leq \frac{1}{2} \sum_{r=0}^{+\infty} \sqrt{\frac{e^{-(I_p \lambda_s + \lambda_b)} (I_p \lambda_s + \lambda_b)^r}{r!} \frac{e^{-(I_{p'} \lambda_s + \lambda_b)} (I_{p'} \lambda_s + \lambda_b)^r}{r!}} \\ &= \frac{1}{2} e^{-\lambda_b} e^{-\frac{(I_p + I_{p'}) \lambda_s}{2}} \sum_{r=0}^{+\infty} \frac{1}{r!} \left[(I_p \lambda_s + \lambda_b)(I_{p'} \lambda_s + \lambda_b) \right]^{\frac{r}{2}}, \end{aligned} \tag{38}$$

which, following from $e^x = \sum_{n=0}^{+\infty} \frac{x^n}{n!}$ and after straightforward derivations, results in:

$$\Pr(s_{p,1} \to s_{p',1}) \leq \frac{1}{2} e^{-\frac{1}{2} \left(\sqrt{I_p \lambda_s + \lambda_b} - \sqrt{I_{p'} \lambda_s + \lambda_b} \right)^2}. \tag{39}$$

Finally, replacing (39) in (36) results in the expression given in (19).

On the other hand, given that the slot index pairwise error probability is the same for any pair of slots following from the symmetry of the PPM constellation, the probability in (13) can be upper-bounded as follows:

$$P_{e|\mathcal{I}}^{(\text{SPPM})}(\mathcal{S}) \leq \frac{M-1}{P}\sum_{p=1}^{P}\Pr(s_{p,m}\rightarrow s_{p,m'}) \quad \forall \quad m'\neq m, \tag{40}$$

where $\Pr(s_{p,m}\rightarrow s_{p,m'})$ stands for the pairwise error probability of deciding in favor of slot m' when the light signal is in slot m conditioned that the aperture p was pulsed (following from the conditioning imposed in (13)). Applying the Bhattacharyya bound [25], [26]:

$$\Pr(s_{p,m}\rightarrow s_{p,m'}) \leq \frac{1}{2}\sum_{r_1=0}^{+\infty}\cdots\sum_{r_M=0}^{+\infty} \sqrt{\prod_{i=1}^{M}\Pr(R_i=r_i|s_{p,m}=1)\prod_{j=1}^{M}\Pr(R_j=r_j|s_{p,m'}=1)}, \tag{41}$$

where, from (3), the condition $s_{p,m}=1$ implies that R_m has a mean of $I_p\lambda_s+\lambda_b$ while the remaining random variables $R_1,\ldots,R_{m-1},R_{m+1},\ldots,R_M$ have a mean of λ_b. Consequently, (41) can be written as:

$$\Pr(s_{p,m}\rightarrow s_{p,m'}) \leq \frac{1}{2}\sum_{r_1=0}^{+\infty}\cdots\sum_{r_M=0}^{+\infty} \sqrt{\frac{e^{-(I_p\lambda_s+\lambda_b)}(I_p\lambda_s+\lambda_b)^{r_m}}{r_m!}\prod_{\substack{i=1\\ i\neq m}}^{M}\frac{e^{-\lambda_b}\lambda_b^{r_i}}{r_i!}}\times \sqrt{\frac{e^{-(I_p\lambda_s+\lambda_b)}(I_p\lambda_s+\lambda_b)^{r_{m'}}}{r_{m'}!}\prod_{\substack{j=1\\ j\neq m'}}^{M}\frac{e^{-\lambda_b}\lambda_b^{r_j}}{r_j!}}. \tag{42}$$

The last expression can be further simplified as follows:

$$\Pr(s_{p,m}\rightarrow s_{p,m'}) \leq \frac{1}{2}\sum_{r_1=0}^{+\infty}\cdots\sum_{r_M=0}^{+\infty}\prod_{\substack{i=1\\ i\neq m\ ;\ i\neq m'}}^{M}\frac{e^{-\lambda_b}\lambda_b^{r_i}}{r_i!}\times \sqrt{\frac{e^{-(I_p\lambda_s+\lambda_b)}(I_p\lambda_s+\lambda_b)^{r_m}}{r_m!}\frac{e^{-\lambda_b}\lambda_b^{r_{m'}}}{r_{m'}!}}\times \sqrt{\frac{e^{-(I_p\lambda_s+\lambda_b)}(I_p\lambda_s+\lambda_b)^{r_{m'}}}{r_{m'}!}\frac{e^{-\lambda_b}\lambda_b^{r_m}}{r_m!}}. \tag{43}$$

Observing that the summations over r_i for $i\neq m$ and $i\neq m'$ are equal to 1, (43) simplifies to:

$$\Pr(s_{p,m}\rightarrow s_{p,m'}) \leq \frac{1}{2}e^{-\lambda_b}e^{-(I_p\lambda_s+\lambda_b)} \sum_{r_m=0}^{+\infty}\frac{1}{r_m!}[\lambda_b(I_p\lambda_s+\lambda_b)]^{\frac{r_m}{2}}\sum_{r_{m'}=0}^{+\infty}\frac{1}{r_{m'}!}[\lambda_b(I_p\lambda_s+\lambda_b)]^{\frac{r_{m'}}{2}}, \tag{44}$$

which, following from $e^x=\sum_{n=0}^{+\infty}\frac{x^n}{n!}$ and after straightforward derivations, results in:

$$\Pr(s_{p,m}\rightarrow s_{p,m'}) \leq \frac{1}{2}e^{-\left(\sqrt{I_p\lambda_s+\lambda_b}-\sqrt{\lambda_b}\right)^2}. \tag{45}$$

Finally, replacing (45) in (40) results in the expression given in (20).

Appendix B

For large values of λ_s and $\lambda_b\rightarrow 0$, the upper-bound in (21) can be determined from:

$$\begin{aligned} P_e^{(\text{OSSK})} &= \frac{P-1}{2}\int_0^{+\infty}\int_0^{+\infty}e^{-\frac{\lambda_s}{2}\left(\sqrt{x}-\sqrt{y}\right)^2}f_X(x)f_Y(y)\mathrm{d}x\mathrm{d}y \\ &= \frac{P-1}{2}\int_0^{+\infty}e^{-\frac{\lambda_s}{2}z}f_{(\sqrt{X}-\sqrt{Y})^2}(z)\mathrm{d}z. \end{aligned} \tag{46}$$

Since the integral in (46) is dominated by small values of z, we next determine the distribution $f_{(\sqrt{X}-\sqrt{Y})^2}(z)$ for $z\ll 1$ where X and Y are two independent and identically-distributed gamma-gamma random variables according to (1).

First, we evaluate the distribution $f_{\sqrt{X}-\sqrt{Y}}(z)$. Using standard random variable transformation techniques, the cumulative distribution function (cdf) of the random variable $Z=\sqrt{X}-\sqrt{Y}$ is $F_Z(z)=\Pr(Z\leq z)=\Pr(\sqrt{X}-\sqrt{Y}\leq z)=\Pr(\sqrt{Y}\geq\sqrt{X}-z)$. This cdf can be evaluated using $F_Z(z)=\int_{-\infty}^{+\infty}\int_{x-z}^{+\infty}f_{\sqrt{X}}(x)f_{\sqrt{Y}}(y)\mathrm{d}y\mathrm{d}x$. Differentiating with respect to z using the Leibniz integral rule results in $f_Z(z)=\frac{\mathrm{d}F_Z(z)}{\mathrm{d}z}=\int_{-\infty}^{+\infty}f_{\sqrt{X}}(x)f_{\sqrt{Y}}(x-z)\mathrm{d}x$. Given that the random variables $\sqrt{X}$ and $\sqrt{Y}$ assume positive values, then $f_{\sqrt{X}}(x)f_{\sqrt{Y}}(x-z)$ is nonzero for $x\geq\max\{0,z\}$. As will be explained later, $f_Z(z)$ needs to be evaluated only for $z\leq 0$:

$$f_{\sqrt{X}-\sqrt{Y}}(z)=\int_0^{+\infty}f_{\sqrt{X}}(x)f_{\sqrt{Y}}(x-z)\mathrm{d}x \quad ; \quad z\leq 0. \tag{47}$$

In order to be able to solve the challenging integral in (47), the gamma-gamma pdf in (1) will be written under the form of a mixture gamma (MG) distribution based on [27], [28]:

$$f_X(x)=x^{\beta-1}\sum_{i=1}^{N}a_ie^{-b_ix} \quad ; \quad x\geq 0, \tag{48}$$

where the constants a_i and b_i can be determined from equation (4) in [28] while the number of terms N determines the level of accuracy of the approximation [27]. The reason behind adopting the MG distribution stems from the fact that (47) calls for the multiplication of two shifted versions of the square root gamma-gamma pdf, thus necessitating an approximation that holds for all values of the irradiance rather than for small values only.

Since $f_{\sqrt{X}}(x)=2xf_X(x^2)$, then replacing (48) in (47) results in:

$$f_{\sqrt{X}-\sqrt{Y}}(z)=4\sum_{i=1}^{N}\sum_{j=1}^{N}a_ia_j\times \int_0^{+\infty}x^{2\beta-1}e^{-b_ix^2}(x-z)^{2\beta-1}e^{-b_j(x-z)^2}\mathrm{d}x \ ; \ z\leq 0, \tag{49}$$

$$f_{\sqrt{X}-\sqrt{Y}}(z)=4\sum_{i=1}^{N}\sum_{j=1}^{N}\sum_{k=0}^{+\infty}a_i a_j\binom{2\beta-1}{k}e^{-b_j z^2}(-z)^k[4(b_i+b_j)]^{\frac{k+1-4\beta}{2}}\Gamma(4\beta-k-1)\sqrt{\pi}$$
$$\left[\frac{1}{\Gamma\left(\frac{4\beta-k}{2}\right)}\Phi\left(\frac{4\beta-k-1}{2},\frac{1}{2};\frac{b_j^2}{b_i+b_j}z^2\right)+\frac{2b_j z}{\sqrt{b_i+b_j}\Gamma\left(\frac{4\beta-k-1}{2}\right)}\Phi\left(\frac{4\beta-k}{2},\frac{3}{2};\frac{b_j^2}{b_i+b_j}z^2\right)\right]. \quad (51)$$

which, following from the generalized binomial theorem, can be expanded as follows:

$$f_{\sqrt{X}-\sqrt{Y}}(z)=4\sum_{i=1}^{N}\sum_{j=1}^{N}\sum_{k=0}^{+\infty}a_i a_j\binom{2\beta-1}{k}e^{-b_j z^2}(-z)^k\times$$
$$\int_0^{+\infty}x^{4\beta-2-k}e^{-(b_i+b_j)x^2}e^{2b_j zx}\mathrm{d}x\ ;\ z\leq 0. \quad (50)$$

Solving the integral in (50) using [31, 3.462.2] while relating the obtained parabolic cylinder function to the confluent hypergeometric function using [31, 9.240] results in (51) shown on top of the page.

For small values of $|z|$, $\Phi(\alpha,\gamma;z)\to 1$ following from [31, 9.210.1]. Therefore, setting $k=0$ in (51) while ignoring the higher powers of z for $|z|\ll 1$ results in:

$$f_{\sqrt{X}-\sqrt{Y}}(z)\approx 4\frac{\Gamma(4\beta-1)\sqrt{\pi}}{\Gamma(2\beta)}\times$$
$$\sum_{i=1}^{N}\sum_{j=1}^{N}a_i a_j([4(b_i+b_j)]^{\frac{1-4\beta}{2}}e^{-b_j z^2}$$
$$\triangleq\sum_{l}\chi_l e^{-\zeta_l z^2}\ \ ;\ \ z\leq 0. \quad (52)$$

On the other hand, $f_{(\sqrt{X}-\sqrt{Y})^2}(z)=\frac{1}{2\sqrt{z}}\left[f_{\sqrt{X}-\sqrt{Y}}(\sqrt{z})+f_{\sqrt{X}-\sqrt{Y}}(-\sqrt{z})\right]$. Since the function $f_{\sqrt{X}-\sqrt{Y}}(z)$ is even following from the fact that X and Y are identically-distributed, then the last relation simplifies to $f_{(\sqrt{X}-\sqrt{Y})^2}(z)=\frac{1}{\sqrt{z}}f_{\sqrt{X}-\sqrt{Y}}(-\sqrt{z})$. Now, since $-\sqrt{z}\leq 0$, then (52) can be applied resulting in $f_{(\sqrt{X}-\sqrt{Y})^2}(z)=\frac{1}{\sqrt{z}}\sum_l\chi_l e^{-\zeta_l z}$ for $z\geq 0$. Therefore, the SEP in (46) can be evaluated as follows:

$$P_e^{(\mathrm{OSSK})}=\frac{P-1}{2}\sum_l\chi_l\int_0^{+\infty}\frac{1}{\sqrt{z}}e^{-\left(\frac{\lambda_s}{2}+\zeta_l\right)z}\mathrm{d}z$$
$$=\frac{P-1}{2}\sum_l\chi_l\sqrt{\frac{\pi}{\frac{\lambda_s}{2}+\zeta_l}}, \quad (53)$$

where the second equality follows from [31, 3.361.2]. For large values of λ_s, $P_e^{(\mathrm{OSSK})}\to(P-1)\sqrt{\frac{\pi}{2}}(\sum_l\chi_l)\lambda_s^{-\frac{1}{2}}$ implying that the diversity order is equal to $1/2$.

Appendix C

For large values of λ_s and $\lambda_b\to 0$, the upper-bound in (22) can be determined from:
$P_e^{(\mathrm{SPPM})}(\mathcal{S})=\frac{M-1}{2}\int_0^{+\infty}e^{-\lambda_s x}f_X(x)\mathrm{d}x$. Approximating the gamma-gamma pdf in (1) by the first term of the power series expansion near the origin results in $f_X(x)\approx ax^{\beta-1}$ where $a=\frac{\Gamma(\alpha-\beta)}{\Gamma(\alpha)\Gamma(\beta)}(\alpha\beta)^\beta$ [29]. Solving the obtained integral results in $P_e^{(\mathrm{SPPM})}(\mathcal{S})=\frac{(M-1)a\Gamma(\beta)}{2}\lambda_s^{-\beta}$ implying that the diversity order is equal to β and completing the proof of proposition 3.

Appendix D

For $\lambda_s\gg 1$ and $\lambda_b\to 0$, the integral in (26) can be calculated from:

$$I\triangleq\int_0^{+\infty}\int_0^{y}e^{-\frac{\lambda_s}{2}(y-x)^2}f_{\sqrt{I_p},\sqrt{I_{p'}}}(x,y)\mathrm{d}x\mathrm{d}y, \quad (54)$$

where the joint pdf of the p-th and p'-th order statistics ($p<p'$) is given by [30, 2.3.2]:

$$f_{\sqrt{I_p},\sqrt{I_{p'}}}(x,y)=\frac{P!}{(p-1)!(p'-p-1)!(P-p')!}\times$$
$$f_{\sqrt{X}}(x)f_{\sqrt{Y}}(y)\left[F_{\sqrt{X}}(x)\right]^{p-1}\left[F_{\sqrt{Y}}(y)-F_{\sqrt{X}}(x)\right]^{p'-p-1}\times$$
$$\left[1-F_{\sqrt{Y}}(y)\right]^{P-p'}\ \ ;\ \ 0\leq x\leq y, \quad (55)$$

where $f_{\sqrt{X}}(x)=2xf_X(x^2)$ and $F_{\sqrt{X}}(x)=F_X(x^2)$ correspond to the pdf and cdf of the square-root of a gamma-gamma random variable whose pdf $f_X(x)$ is given in (1).

Now, consider the random variable $\sqrt{I_{p'}}-\sqrt{I_p}$ that assumes only positive values since $I_p\leq I_{p'}$. In terms of this random variable, (54) can be evaluated as follows:

$$I=\int_0^{+\infty}e^{-\frac{\lambda_s}{2}z^2}f_{\sqrt{I_{p'}}-\sqrt{I_p}}(z)\mathrm{d}z. \quad (56)$$

The cdf of the random variable $Y-X$ with $Y=\sqrt{I_{p'}}$ and $X=\sqrt{I_p}$ can be calculated from $F_{Y-X}(z)=\Pr(Y-X\leq z)$ which, when combined with the relation $0\leq X\leq Y$, results in $F_{Y-X}(z)=\int_0^{+\infty}\int_x^{x+z}f_{X,Y}(x,y)\mathrm{d}y\mathrm{d}x$. Differentiating with respect to z using the Leibniz integral rule results in $f_{Y-X}(z)=\int_0^{+\infty}f_{X,Y}(x,x+z)\mathrm{d}x$. Therefore, the pdf needed for the evaluation of (56) can be determined from (55) as:

$$f_{\sqrt{I_{p'}}-\sqrt{I_p}}(z)=\int_0^{+\infty}f_{\sqrt{I_p},\sqrt{I_{p'}}}(x,x+z)\mathrm{d}x\ ;\ z\geq 0. \quad (57)$$

Since the small values of z contribute the most to the integral in (56), we next evaluate the pdf in (57) for small values of z. Replacing y by $x+z$ in (55), a key point in the proof consists of observing that $F_{\sqrt{Y}}(y)-F_{\sqrt{X}}(x)=z\frac{F_{\sqrt{X}}(x+z)-F_{\sqrt{X}}(x)}{z}\to z\frac{\mathrm{d}F_{\sqrt{X}}(x)}{\mathrm{d}x}=zf_{\sqrt{X}}(x)$ as $z\to 0$. Therefore, for small values of z:

$$f_{\sqrt{I_p},\sqrt{I_{p'}}}(x,x+z)=cz^{p'-p-1}\sum_{l=0}^{P-p'}\binom{P-p'}{l}(-1)^l\times$$
$$\left[f_{\sqrt{X}}(x)\right]^{p'-p}f_{\sqrt{X}}(x+z)\left[F_{\sqrt{X}}(x)\right]^{p-1}\left[F_{\sqrt{X}}(x+z)\right]^{l}, \quad (58)$$

$$f_{\sqrt{I_p},\sqrt{I_{p'}}}(x,x+z)=c2^{p'-p+1}[\Gamma(\beta)]^{p-1}z^{p'-p-1}\sum_{l=0}^{P-p'}\binom{P-p'}{l}[-\Gamma(l)]^l\sum_{i_1=1}^{N}\cdots\sum_{i_{p'-p}=1}^{N}\sum_{i'=1}^{N}$$
$$\sum_{i_1''=1}^{N}\cdots\sum_{i_{p-1}''=1}^{N}\sum_{i_1'''=1}^{N}\cdots\sum_{i_l'''=1}^{N}\sum_{k_1=0}^{+\infty}\cdots\sum_{k_{p-1}=0}^{+\infty}\sum_{k_1'=0}^{+\infty}\cdots\sum_{k_l'=0}^{+\infty}[a_{i_1}\cdots a_{i_{p'-p}}]a_{i'}[a_{i_1''}\cdots a_{i_{p-1}''}][a_{i_1'''}\cdots a_{i_l'''}]$$
$$\frac{\left[b_{i_1''}^{k_1}\cdots b_{i_{p-1}''}^{k_{p-1}}\right]\left[b_{i_1'''}^{k_1'}\cdots b_{i_l'''}^{k_l'}\right]}{[\Gamma(\beta+k_1+1)\cdots\Gamma(\beta+k_{p-1}+1)]\,[\Gamma(\beta+k_1'+1)\cdots\Gamma(\beta+k_l'+1)]}x^{2\left[(p'-1)\beta+(k_1+\cdots+k_{p-1})+\frac{p-p'+1}{2}\right]-1}$$
$$e^{-\left[(b_{i_1}+\cdots+b_{i_{p'-p}})+(b_{i_1''}+\cdots+b_{i_{p-1}''})\right]x^2}(x+z)^{2\left[(l+1)\beta+(k_1'+\cdots+k_l')\right]-1}e^{-\left[b_{i'}+(b_{i_1'''}+\cdots+b_{i_l'''})\right](x+z)^2}. \quad (62)$$

where $c\triangleq\frac{P!}{(p-1)!(p'-p-1)!(P-p')!}$.

As in Appendix B, the versatile mixture gamma (MG) distribution will be used to approximate the gamma-gamma distribution [27], [28]:

$$f_X(x)=x^{\beta-1}\sum_{i=1}^{N}a_ie^{-b_ix}$$
$$\Rightarrow\ F_X(x)=\sum_{i=1}^{N}\frac{a_i}{b_i^\beta}\gamma(\beta,b_ix)\ \ ;\ \ x\geq 0, \quad (59)$$

where $\gamma(s,x)$ stands for the lower incomplete gamma function while the constants a_i and b_i can be determined from equation (4) in [28]. Equation (59) implies that (for $x\geq 0$):

$$f_{\sqrt{X}}(x)=2x^{2\beta-1}\sum_{i=1}^{N}a_ie^{-b_ix^2} \quad (60)$$

$$F_{\sqrt{X}}(x)=\sum_{i=1}^{N}\frac{a_i}{b_i^\beta}\gamma(\beta,b_ix^2)$$
$$=\Gamma(\beta)x^{2\beta}\sum_{i=1}^{N}a_ie^{-b_ix^2}\sum_{k=0}^{+\infty}\frac{(b_ix^2)^k}{\Gamma(\beta+k+1)}, \quad (61)$$

where the last relation follows from the power series expansion of the lower incomplete gamma function. Replacing (60) and (61) in (58) results in (62) shown on top of the page:

For simplicity of notation, (62) can be written under the following form:

$$f_{\sqrt{I_p},\sqrt{I_{p'}}}(x,x+z)=z^{p'-p-1}\times$$
$$\sum_m\chi_mx^{2\mu_m-1}(x+z)^{2\nu_m-1}e^{-\gamma_mx^2}e^{-\zeta_m(x+z)^2}. \quad (63)$$

Applying the binomial theorem on (63) and replacing in (57) results in:

$$f_{\sqrt{I_{p'}}-\sqrt{I_p}}(z)=\sum_{k=0}^{+\infty}\sum_m\binom{2\nu_m-1}{k}\chi_mz^{p'-p-1+k}e^{-\zeta_mz^2}$$
$$\int_0^{+\infty}x^{2(\mu_m+\nu_m-1)-k}e^{-(\gamma_m+\zeta_m)x^2}e^{-2\zeta_mzx}\mathrm{d}x\ ;\ z\geq 0. \quad (64)$$

The integral in (64) has the same form as the integral in (50). Therefore, following a similar analysis as the one presented in Appendix B (in particular (51) and the subsequent approximations), it can be proven that the former integral behaves like a constant as a function of z for $z\ll 1$. Denoting this constant by ψ_m while approximating the summation in (64) by the smallest term $k=0$ (corresponding to the smallest power of z) results in:

$$f_{\sqrt{I_{p'}}-\sqrt{I_p}}(z)\approx z^{p'-p-1}\sum_m\chi_m\psi_me^{-\zeta_mz^2}\ \ ;\ \ z\geq 0. \quad (65)$$

Replacing (65) in (56) results in: $I=\sum_m\chi_m\psi_m\int_0^{+\infty}z^{p'-p-1}e^{-\left(\frac{\lambda_s}{2}+\zeta_m\right)z^2}\mathrm{d}z$. This integral can be solved using [31, 3.462.9]:

$$I=\frac{1}{2}\Gamma\left(\frac{p'-p}{2}\right)\sum_m\chi_m\psi_m\left(\frac{\lambda_s}{2}+\zeta_m\right)^{-\frac{p'-p}{2}}$$
$$\to 2^{\frac{p'-p}{2}-1}\Gamma\left(\frac{p'-p}{2}\right)\lambda_s^{-\frac{p'-p}{2}}\sum_m\chi_m\psi_m, \quad (66)$$

showing that the diversity order is equal to $\frac{p'-p}{2}$ (for $p<p'$).

Appendix E

For $\lambda_s\gg 1$ and $\lambda_b\to 0$, the integral in (27) can be written as $I\triangleq\int_0^{+\infty}e^{-\lambda_sx}f_{I_p}(x)\mathrm{d}x$. Based on order statistics, the pdf of p-th smallest random variable I_p is given by [30, 2.2.2]:

$$f_{I_p}(x)=\frac{P!}{(p-1)!(P-p)!}f_X(x)\left[F_X(x)\right]^{p-1}\left[1-F_X(x)\right]^{P-p}, \quad (67)$$

where $f_X(x)$ corresponds to the gamma-gamma pdf in (1) while $F_X(x)$ stands for the corresponding cdf. Approximating these functions by the first term of their corresponding power series expansions near the origin $f_X(x)=ax^{\beta-1}$ and $F_X(x)=\frac{a}{\beta}x^\beta$ (where a is given in Appendix C) results in:

$$f_{I_p}(x)\approx\sum_{k=0}^{P-p}\binom{P-p}{k}(-1)^k\times$$
$$\frac{P!}{(p-1)!(P-p)!}\frac{a^{p+k}}{\beta^{p-1+k}}x^{(p+k)\beta-1}\ ;\ x\ll 1, \quad (68)$$

where this expression can be further approximated by the first term of the summation (corresponding to $k=0$): $f_{I_p}(x)\approx\frac{P!}{(p-1)!(P-p)!}\frac{a^p}{\beta^{p-1}}x^{p\beta-1}$. Replacing this expression in the integral I results in $I\approx\frac{P!}{(p-1)!(P-p)!}\frac{a^p}{\beta^{p-1}}\Gamma(p\beta)\lambda_s^{-p\beta}$ completing the proof.

APPENDIX F

From (29), writing the integer p under the form $p = P - k(P_s-1)$, we observe that the P_s-1 integers $p, p-1, \ldots, p-(P_s-2)$ all result in the same value of $\left\lfloor \frac{P-p}{P_s-1} \right\rfloor = k$. Since, among these integers, the integer p results in the largest value of $p\beta$, then the diversity order in (29) can be written under the form:

$$\delta^{(\text{SPPM})} = \max_k \left\{ [P - k(P_s-1)]\beta, \frac{1}{2}k \right\} \triangleq \max_k \{\delta_k\}. \tag{69}$$

As in the case of OSSK from (31), selecting the aperture indices equidistantly between $p = P-k(P_s-1)$ and P results in the candidate set:

$$\mathcal{C}_k = \{P - k(P_s-1), P - k(P_s-2), \ldots, P\}. \tag{70}$$

Solving for the smallest integer k satisfying:

$$\frac{1}{2}k \leq [P - k(P_s-1)]\beta, \tag{71}$$

results in the solution $k = \tilde{k}$ given in (33). In this context, $\delta_{\tilde{k}} = \frac{1}{2}\tilde{k} \triangleq \delta_1^{(\text{SPPM})}$ and $\delta_{\tilde{k}+1} = [P - (\tilde{k}+1)(P_s-1)]\beta \triangleq \delta_2^{(\text{SPPM})}$.

For $k < \tilde{k}$, $\delta_k = \frac{1}{2}k < \frac{1}{2}\tilde{k} = \delta_{\tilde{k}}$. Similarly, for $k > \tilde{k}+1$, $\delta_k = [P - k(P_s-1)]\beta < [P - (\tilde{k}+1)(P_s-1)]\beta = \delta_{\tilde{k}+1}$. Therefore, the values of k that maximize (69) are either $k_{\text{opt}} = \tilde{k}$ with $\delta^{(\text{SPPM})} = \delta_1^{(\text{SPPM})}$ or $k_{\text{opt}} = \tilde{k}+1$ with $\delta^{(\text{SPPM})} = \delta_2^{(\text{SPPM})}$ proving equations (32) and (35). Finally, replacing k by k_{opt} in (70) results in the solution given in (34).

REFERENCES

[1] P. Yang, M. Di Renzo, Y. Xiao, S. Li, and L. Hanzo, "Design guidelines for spatial modulation," *IEEE Commun. Surveys & Tutorials*, vol. 17, no. 1, pp. 6–26, 1st quarter 2015.

[2] P. Yang, Y. Xiao, Y. L. Guan, K. Hari, A. Chockalingam, S. Sugiura, H. Haas, M. Di Renzo, C. Masouros, Z. Liu *et al.*, "Single-carrier SM-MIMO: A promising design for broadband large-scale antenna systems," *IEEE Commun. Surveys & Tutorials*, vol. 18, no. 3, pp. 1687–1716, 3rd quarter 2016.

[3] M. Di Renzo and H. Haas, "Bit error probability of SM-MIMO over generalized fading channels," *IEEE Trans. Veh. Technol.*, vol. 61, no. 3, pp. 1124–1144, Mar. 2012.

[4] K. P. Peppas, M. Zamkotsian, F. Lazarakis, and P. G. Cottis, "Asymptotic error performance analysis of spatial modulation under generalized fading," *IEEE Wireless Commun. Letters*, vol. 3, no. 4, pp. 421–424, Aug. 2014.

[5] R. Rajashekar, K. Hari, and L. Hanzo, "Quantifying the transmit diversity order of Euclidean distance based antenna selection in spatial modulation," *IEEE Signal Processing Lett.*, vol. 22, no. 9, pp. 1434–1437, Sep. 2015.

[6] R. Rajashekar, K. Hari, and L. Hanzo, "Antenna selection in spatial modulation systems," *IEEE Commun. Lett.*, vol. 17, no. 3, pp. 521–524, Mar. 2013.

[7] J. Zheng and J. Chen, "Further complexity reduction for antenna selection in spatial modulation systems," *IEEE Commun. Lett.*, vol. 19, no. 6, pp. 937–940, June 2015.

[8] Z. Sun, Y. Xiao, P. Yang, S. Li, and W. Xiang, "Transmit antenna selection schemes for spatial modulation systems: Search complexity reduction and large-scale MIMO applications," *IEEE Trans. Veh. Technol.*, vol. 66, no. 9, pp. 8010–8021, Sep. 2017.

[9] R. Mesleh, H. Elgala, and H. Haas, "Optical spatial modulation," *IEEE/OSA Journal of Optical Communications and Networking*, vol. 3, no. 3, pp. 234–244, Mar. 2011.

[10] T. Fath and H. Haas, "Performance comparison of MIMO techniques for optical wireless communications in indoor environments," *IEEE Trans. Commun.*, vol. 61, no. 2, pp. 733–742, Feb. 2013.

[11] J.-Y. Wang, J.-X. Zhu, S.-H. Lin, and J.-B. Wang, "Adaptive spatial modulation based visible light communications: SER analysis and optimization," *IEEE Photonics Journal*, vol. 10, no. 3, pp. 1–14, June 2018.

[12] J.-Y. Wang, H. Ge, J.-X. Zhu, J.-B. Wang, J. Dai, and M. Lin, "Adaptive spatial modulation for visible light communications with an arbitrary number of transmitters," *IEEE Access*, vol. 6, pp. 37 108–37 123, July 2018.

[13] A. Yesilkaya, T. Cogalan, E. Panayirci, H. Haas, and H. V. Poor, "Achieving minimum error in MISO optical spatial modulation," in *2018 IEEE Int. Conf. on Commun. (ICC)*, 2018, pp. 1–6.

[14] H. G. Olanrewaju, J. Thompson, and W. O. Popoola, "Performance of optical spatial modulation in indoor multipath channel," *IEEE Trans. Wireless Commun.*, vol. 17, no. 9, pp. 6042–6052, Sep. 2018.

[15] A. Jaiswal, M. R. Bhatnagar, and V. K. Jain, "Performance of optical space shift keying over gamma-gamma fading with pointing error," *IEEE Photonics Journal*, vol. 9, no. 2, pp. 1–16, April 2017.

[16] A. Jaiswal, M. R. Bhatnagar, and V. K. Jain, "Performance evaluation of space shift keying in free-space optical communication," *IEEE/OSA Journal of Optical Communications and Networking*, vol. 9, no. 2, pp. 149–160, Feb. 2017.

[17] A. Jaiswal, M. Abaza, M. R. Bhatnagar, and V. K. Jain, "An investigation of performance and diversity property of optical space shift keying based FSO-MIMO system," *IEEE Trans. Commun.*, vol. 66, no. 9, pp. 4028–4042, Sep. 2018.

[18] T. Özbilgin and M. Koca, "Optical spatial modulation over atmospheric turbulence channels," *J. Lightwave Technol.*, vol. 33, no. 11, pp. 2313–2323, June 2015.

[19] K. P. Peppas and P. T. Mathiopoulos, "Free-space optical communication with spatial modulation and coherent detection over H-K atmospheric turbulence channels," *J. Lightwave Technol.*, vol. 33, no. 20, pp. 4221–4232, Oct. 2015.

[20] S.-H. Hwang and Y. Cheng, "SIM/SM-aided free-space optical communication with receiver diversity," *J. Lightwave Technol.*, vol. 32, no. 14, pp. 2443–2450, July 2014.

[21] S. G. Wilson, M. Brandt-Pearce, Q. Cao, and J. H. Leveque, "Free-space optical MIMO transmission with Q-ary PPM," *IEEE Trans. Commun.*, vol. 53, no. 8, pp. 1402–1412, Aug. 2005.

[22] C. Abou-Rjeily, "Spatial-multiplexing for photon-counting MIMO-FSO communication systems," *IEEE Trans. Wireless Commun.*, vol. 17, no. 9, pp. 5789 – 5803, Sep. 2018.

[23] M. L. Riediger, R. Schober, and L. Lampe, "Multiple-symbol detection for photon-counting MIMO free-space optical communications," *IEEE Trans. Wireless Commun.*, vol. 7, no. 12, pp. 5369–5379, Dec. 2008.

[24] T. Song and P.-Y. Kam, "Robust data detection for the photon-counting free-space optical system with implicit CSI acquisition and background radiation compensation," *J. Lightwave Technol.*, vol. 34, no. 4, pp. 1120–1132, Feb. 2016.

[25] S. B. Wicker, *Error control systems for digital communication and storage*. Prentice hall Englewood Cliffs, 1995, vol. 1.

[26] M. Griot, W.-Y. Weng, and R. D. Wesel, "A tighter Bhattacharyya bound for decoding error probability," *IEEE Commun. Lett.*, vol. 11, no. 4, pp. 1–2, April 2007.

[27] S. Atapattu, C. Tellambura, and H. Jiang, "A mixture gamma distribution to model the SNR of wireless channels," *IEEE Trans. Wireless Commun.*, vol. 10, no. 12, pp. 4193–4203, Dec. 2011.

[28] J. Jung, S.-R. Lee, H. Park, S. Lee, and I. Lee, "Capacity and error probability analysis of diversity reception schemes over generalized-k fading channels using a mixture gamma distribution," *IEEE Trans. Wireless Commun.*, vol. 13, no. 9, pp. 4721–4730, Sep. 2014.

[29] C. Abou-Rjeily, "Performance analysis of FSO communications with diversity methods: Add more relays or more apertures?" *IEEE J. Select. Areas Commun.*, vol. 33, no. 9, pp. 1890 – 1902, Sep. 2015.

[30] B. C. Arnold, N. Balakrishnan, and H. N. Nagaraja, *A First Course in Order Statistics*. Wiley, 1992.

[31] I. Gradshteyn and I. Ryzhik, *Table of integrals, series and products*, 6th ed., 2000.

Chadi Abou-Rjeily is a professor at the department of Electrical and Computer Engineering of the Lebanese American University (LAU), Byblos, Lebanon. He received his BE degree in electrical engineering in 2002 from the Lebanese University, Roumieh, Lebanon. He received his M.S. and Ph.D. degrees in electrical engineering in 2003 and 2006, respectively, from the École Nationale Supérieure des Télécommunications (ENST), Paris, France. From September 2003 to February 2007, he was also a research fellow at the Laboratory of Electronics and Information Technology of the French Atomic Energy Commission (CEA-LETI). His research interests are in the code construction and transceiver design for wireless communication systems.

Georges Kaddoum received the bachelors degree in electrical engineering from the École Nationale Supérieure de Techniques Avancées (ENSTA), France, and the M.S. degree in telecommunications and signal processing from Telecom Bretagne (ENSTB), Brest, in 2005 and the Ph.D. degree in signal processing and telecommunications from the National Institute of Applied Sciences (INSA), Toulouse, France, in 2009. He is currently an Associate Professor and Research chair of electrical engineering with the École de Technologie Supérieure (ETS), University of Quebec, and Montreal, QC, Canada. His recent research activities cover wireless communication networks, resource allocations, security and space communications and navigation.